Post Hatfield rolling contact fatigue

The effect of residual stress on contact stress driven crack growth in rail

Comparison of the Hatfield and alternative UK rails using models to assess the effect of residual stress on crack growth from rolling contact fatigue

DI Fletcher, A Kapoor, FJ Franklin,
L Smith and P Hyde

November 2006

NewRail Report No. WR061106-6

NewRail | School of Mechanical & Systems Engineering | Newcastle University
NE1 7RU | UK | T+44 (0)191 222 5821 |F+44 (0)191 222 5821 | www.newrail.org

OFFICE OF RAIL REGULATION

Contents

Executive summary

Rail decarburisation and crack initiation

The Dynarat "brick" model has been used to simulate a decarburised layer using a hexagonal pattern of "pearlite" grains with (pro-eutectoid) ferrite grain boundaries, where the thickness of the grain boundaries increased towards the surface. This model is used here for prediction of crack initiation and early growth (tens to hundreds of microns).

For the conditions modelled, the presence of a decarburised layer is predicted to produce a peak depth to which cracks may initiate of up to $340 - 380\mu$m. The comparable depth for a non-decarburised steel was found to be $5 - 10\mu$m, indicating that the decarburisation has led to around a thirty times increase in the size of cracks which may initiate by ratchetting plasticity accumulation, prior to the removal of the decarburised layer by wear.

The decarburised layer is predicted to wear rapidly under the specific conditions modelled. A limited set of crack growth modelling cases shows that the initiated cracks will be worn out before they become established as long cracks driven by contact and residual stresses. However, further modelling would be required to determine the longer term influence of a decarburised layer, beyond the rapid crack initiation period over a wider range of conditions, for example higher friction dry contact conditions. Influences on the overall effect of decarburisation will include the rapid increase in rail-wheel profile conformity and consequent contact pressure drop brought about by wear of the decarburised surface.

Residual stress and long crack growth modelling

To increase confidence in the results produced by the "2.5d" crack growth model three stages of validation using alternative models have been undertaken. These models are used for calculation of growth rate and branching direction for cracks in the millimetre size range.

- First, the output of the "2.5d" model without residual stress applied was compared to published data from an alternative model, showing good agreement in the results. Most importantly, the trends predicted by both models with surface and crack face friction are identical.
- Second, again without residual stress applied, a fully three dimensional boundary element model was created (using the Beasy boundary element modelling software) for growth of an inclined crack in a rail. The comparison of its results with those of the 2.5d model showed that the forms of mode I (opening) and mode II (shearing) results were very similar for the two modelling methods. This indicates that the boundary element model is working well, and that the presence of friction between the crack faces has been captured.
- Third, residual stress was added to the boundary element model. The agreement found between the boundary element and 2.5d models indicates that trends in crack growth predicted using the 2.5d model will be very close to those which could be predicted by further runs of the fully

three dimensional boundary element model. There were some differences between the models in mode I (opening) stress intensity factor results, and in the static values of stress intensity factor present when the wheel contact is remote from the crack. Further research is required to fully understand these differences, although the results of the two independently created models were in generally good agreement considering the complexity of the contact and residual stress regime being modelled.

This report contains revised information on the residual stress input data, and supersedes earlier versions of the report.

1 Introduction

Recent work [1, 2, 3, 4, 5, 6] conducted to investigate the effect of residual stress on the growth of surface breaking rolling contact fatigue cracks has centred on two themes: (1) modelling of the effect of rail residual stress on rolling contact fatigue crack growth and crack branching, and (2) experimental investigation of the effect of rail surface decarburisation on crack initiation.

This report continues from the previous work, and details modelling conducted to develop a comparison of Hatfield and alternative rail steels through examination of the effect of decarburisation on crack initiation. The input data on decarburisation comes from both the experimental data collected in the previous investigations, and alternative data available from published literature.

Also included in this report is validation work on the hybrid two and three dimensional fracture mechanics based crack growth model ("2.5d" model) used in work conducted previously [1, 2, 3, 4, 5, 6] to predict the effect of residual stress on crack growth. This validation has been conducted using newly developed fully three dimensional models, but could not be based on Hatfield specific rail residual stress data because this was not available. Use of alternative input data does not affect this validation, since examination of agreement between models is independent of the residual stress profiles used, providing that the same profiles are used in both modelling approaches.

2 Modelling the effect of decarburisation on crack initiation

2.1 Ratcheting strain decarburisation model

The very earliest stages of crack growth in the rail are driven primarily by accumulation of plasticity in the surface layers of the rail. This plasticity accumulates with each wheel pass (a ratchetting process) until the material is unable to sustain further deformation and fails as it reaches its "limit of ductility" [7]. Cracks at this stage are too small for their growth to be described by the fracture mechanics models applicable to longer cracks. Instead, the presence of adjacent regions of failed, i.e. ductility exhausted, material can be used as an indicator of the presence of cracks. Such failed material will still be able to sustain compression, just as a crack can when its faces are pressed shut. Also, just as a crack cannot sustain shear or tension moving its faces apart, neither can material which has reached the limit of ductility. Material in this condition close to the surface will simply be lost as wear debris, while material held within the rail by adjacent less severely damage material will form weak crack like paths (Figure 1).

Differences in the development of early stage plasticity driven cracks between the normal and decarburised microstructures can be investigated using models based on damage through accumulation of plastic deformation, such as the Dynarat model described below, also known as the "brick" model, which is described in detail in Refs [8] and [9].

Application of the Dynarat model requires its calibration with suitable materials data. Results from twin-disc tests by Carroll and Beynon [10] on decarburised rail disc samples along with twin-disc tests by Garnham et al. [11] on

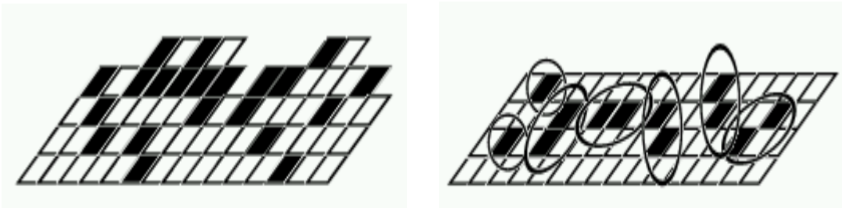

(a) (b)

Figure 1: Rail microstructure cross-sections close to the running surface, divided into an array of 1μm square "bricks", each with physical properties representing the microstructure of the steel at that point. Following wheel contacts and plastic strain accumulation, failed "bricks" within the rail microstructure are shown black. (a) Failed bricks close to the surface are lost as wear debris. (b) Adjacent failed bricks within the body of the rail form weak crack like paths through the microstructure, indicating crack initiation (curved lines enclose adjacent failed bricks).

three types of pearlite rail disc specimens with different amounts of pro-eutectoid ferrite have been used to calibrate the Dynarat model.

2.2 The "brick" model

A cross-section through a rail or rail disc, parallel with the direction of traction, is modelled as a mesh of elements (or "bricks"). In twin-disc contact, the direction of traction is opposite to the direction of motion when the wheel disc is run faster (to simulate a driving wheel). With each load cycle (i.e., wheel pass), each element is subject to a cycle to stress; if the stress is great enough, there will be increment of plastic shear strain. The elements accumulate shear strain over thousands of cycles, and eventually fail when they reach a critical value. This process is illustrated for a rail disc in Figure 2.

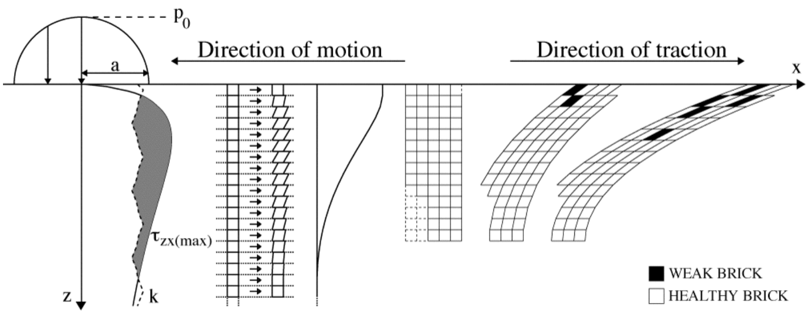

Figure 2: A cross-section through the rail disc modelled as a mesh of elements (or "bricks") subject to a repeated cycle of stress. The elements accumulate shear strain over thousands of cycles, and eventually fail when they reach a critical value. When an element fails, it is described as "weak".

Each element is assigned material properties individually, in particular initial hardness and the critical strain at which failure occurs. These properties are assigned according to a hexagonal pattern which represents a pearlitic steel microstructure of "pearlite" grains and "ferrite" grain boundaries (shown in Figure 3). In reality, each grain in a pearlitic microstructure is a collection of pearlite colonies, and these consist of lamellae of ferrite and cementite. In the model used here, a material called "pearlite" is used to represent this.

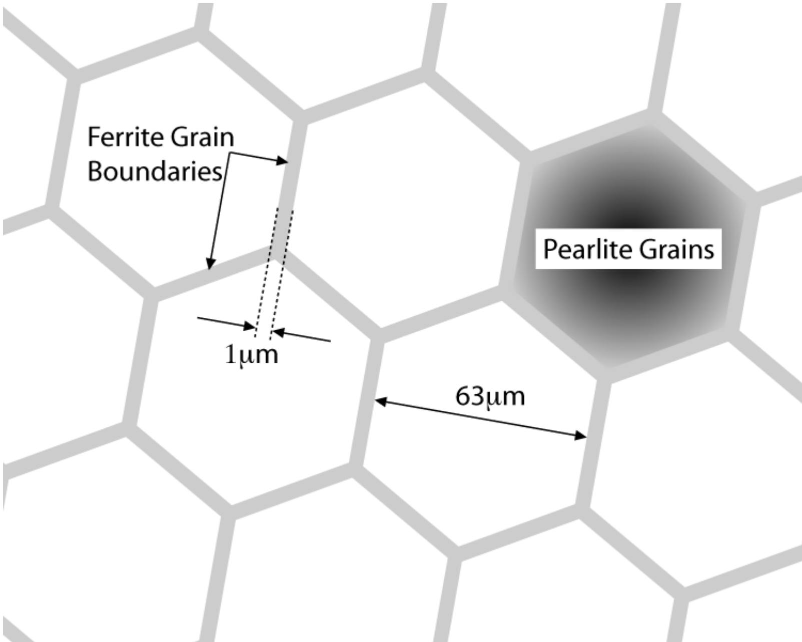

Figure 3: A hexagonal microstructure of "pearlite" grains with "ferrite" grain boundaries. The microstructure is orientated at 10° to the surface.

To represent a decarburised layer, the thickness of the grain boundaries is increased towards the surface. At depths greater than 0.6mm, the grain boundary thickness is 1μm (equal to the size of the elements). This is increased linearly towards the surface, so that the grain boundary thickness is 51μm (i.e., 80% of 64μm) at the surface. Snap shots of the simulated microstructure are given in Figure 4.

The choices of 0.6mm decarburisation depth and grain boundary thickness correspond to the microhardness measurements of the decarburised layer of Sample DE28 in Figure 14 of Ref. [10], reproduced here as Figure 5. The initial hardnesses for "pearlite" and "ferrite" are 370kgf/mm^2 and 250kgf/mm^2 respectively, based on nanohardness measurements from Ref.[11]; these have been normalised so that the equivalent microhardness at depths below the decarburised layer is 242HV0.1 (to match [10]). For both materials, the critical shear strain for failure is 11.

2.3 Results

To illustrate the effect of decarburisation on the microstructure wheel-rail contact is represented here as an elliptic contact patch of transverse and longitudinal half-widths 3mm and 7mm respectively; the peak contact pressure is 1375MPa

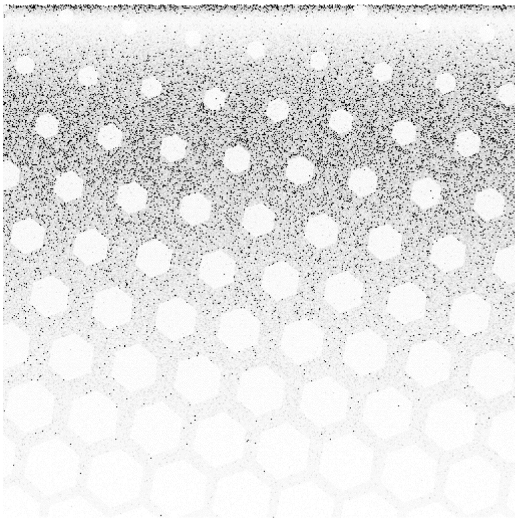

(a)

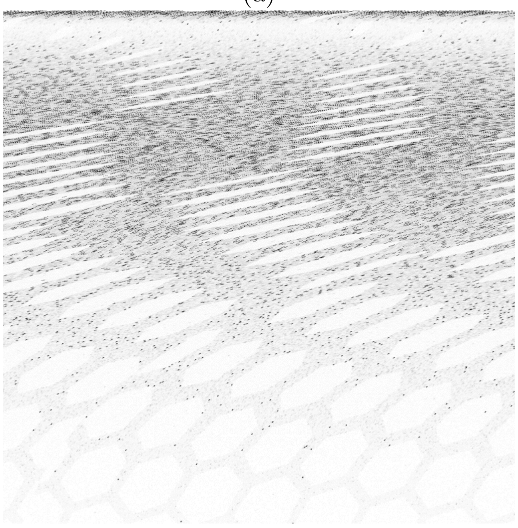

(b)

Figure 4: Images of the simulated decarburised hexagonal microstructure after a total of 10,000 cycles of twin-disc contact. Shown (a) without and (b) with shear strain. The darkness of grey indicated how much shear strain has accumulated; since this is greater in the ferrite, the grain boundaries appear dark while the mostly undeformed 'pearlite' grains appear white.

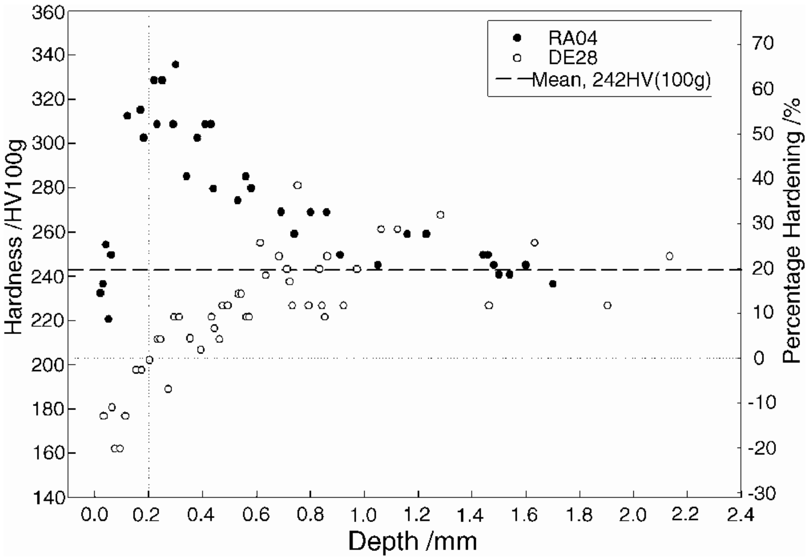

Fig. 14. Microhardness of decarburised rail disc, RA04. The percentage hardening is the increase from the reference sample, DE28, at a depth of 0.2 mm.

Figure 5: Hardness data on decarburised rail steel before and after testing on the SUROS twin disc machine. Reproduced from [10].

and the traction coefficient is 0.33. (The contact is assumed to be fully slipping, so that the friction coefficient is also 0.33.). In later simulations (below), contact conditions for specific positions on the Hatfield curve have been used.

The effect of the decarburised layer on the wear rate of the rail over the first 500,000 cycles (wheel passes) is shown in Figure 6. The wear rate is significantly higher as a result of the decarburisation, peaking at 2.5nm/cycle after 50,000 cycles (compared to 0.5nm/cycle for a rail without decarburisation); the wear rate drops gradually after this until, after 400,000 cycles (by which point the 0.6mm-thick decarburised layer has been worn away completely), it is the same as for a rail without decarburisation.

The profile of microhardness with depth for the simulated rail cross-section is given in Figure 7(a) for a rail with a decarburised layer, and in Figure 7(b) for a rail without a decarburised layer. In both cases the initial profile, i.e., prior to any traffic, is shown. For the rail with a decarburised layer, the average hardness is constant (242HV0.1) outside the decarburised layer (at depths greater than 0.6mm); similarly, for the rail without a decarburised layer, the average hardness is constant (242HV0.1 again) everywhere. Within the decarburised layer, the average hardness increases roughly linearly from 170HV0.1 at the surface to 242HV0.1 at 0.6mm; the hardness corresponds to the ratio of pearlite to ferrite, which is lowest at the surface of the decarburised layer.

Hardness profiles are shown also after 50,000 and 500,000 cycles. For the rail without a decarburised layer, these profiles are almost identical. For the rail

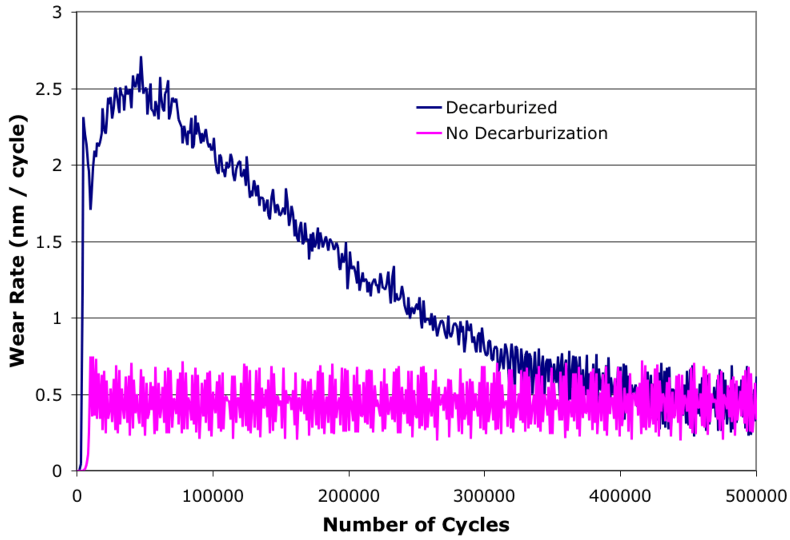

Figure 6: Comparison of wear rates over first 500,000 cycles (wheel passes) for rails with and without a decarburised layer.

with a decarburised layer, the decarburised layer is removed completely after about 400,000 cycles and the hardness profile at 500,000 cycles is identical to the hardness profile at 500,000 cycles for the rail without a decarburised layer.

After only 50,000 cycles, however, the decarburised layer has a clear effect on the hardness profile; for example, the hardness within 100 microns of the surface is only 320HV0.1 compared to 350HV0.1 (or greater) for a rail without decarburisation.

The microstructure consists of pearlite grains and ferrite grain boundaries; since the ferrite is relatively soft compared to the pearlite, the ferrite accumulates shear strain faster and reaches the critical shear strain at which failure occurs sooner. Material which has failed is material in which crack initiation is likely, or through which crack propagation will be rapid.

A key indicator of the likelihood of crack initiation, therefore, is the accumulated shear strain of the ferrite within the microstructure, and this is shown in Figure 8. The shear strain is highest (9-10) at the surface but still less than the critical value (11); the shear strain decreases linearly to 4-5 at a depth of 0.5mm. (This contrasts with results of twin-disc simulations. For twin-disc contact, where the semi-contact width is 0.3mm, the subsurface stresses peak at depths in the range 0.12-0.20mm, i.e., within the decarburised layer. For wheel-rail contact, the subsurface stresses occur deeper within the rail, away from the decarburised layer. The effect of the decarburised layer on twin-disc fatigue life is likely, therefore, to be significantly greater than its effect on rail fatigue life.)

The values of shear strain plotted in Figure 8 have been averaged over the width of the simulation. Because the material properties vary from element to element, some will be relatively weak and can fail even when the average shear strain is quite low. Since a certain percentage of bricks at a depth may fail, even

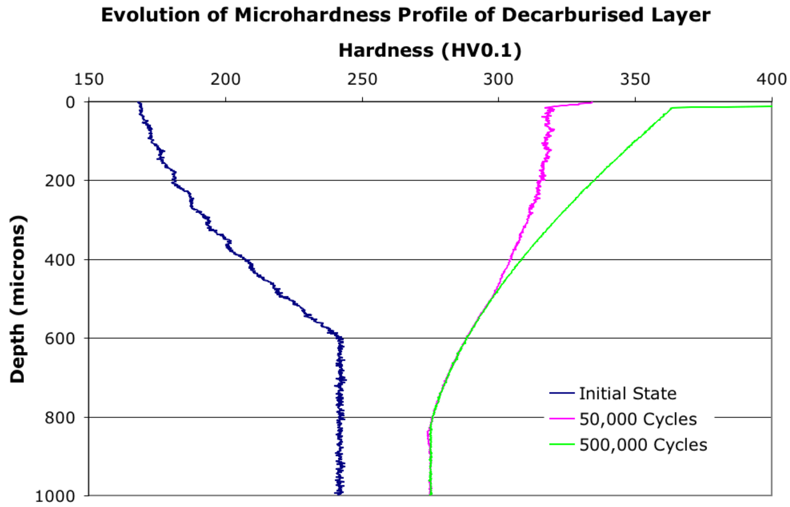

(a)

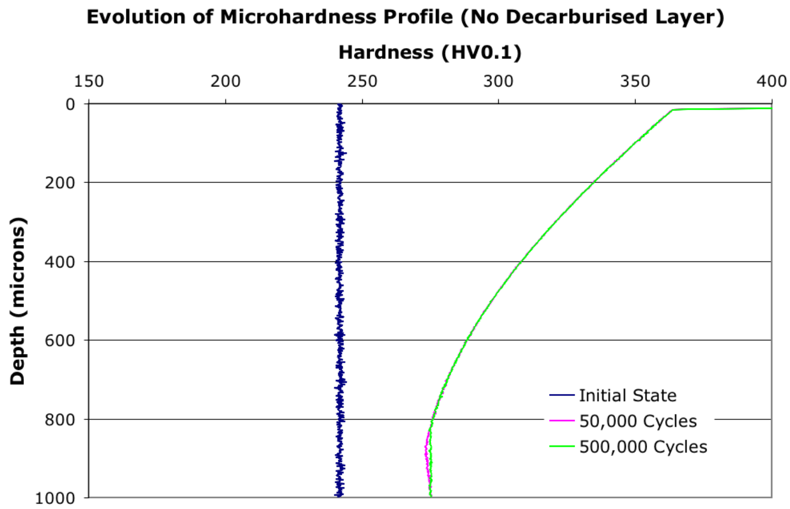

(b)

Figure 7: Hardness profile with depth for a rail (a) with a decarburised layer of thickness 0.6mm, and (b) without a decarburised layer. The initial state (i.e., a new rail) is shown, along with hardness profiles after 50,000 cycles and after 500,000 cycles. After 500,000 cycles, the decarburised layer has worn away and the hardness profile is identical for (a) and (b). Without decarburisation, the profile at 50,000 cycles is almost identical to the profile at 500,000 cycles.

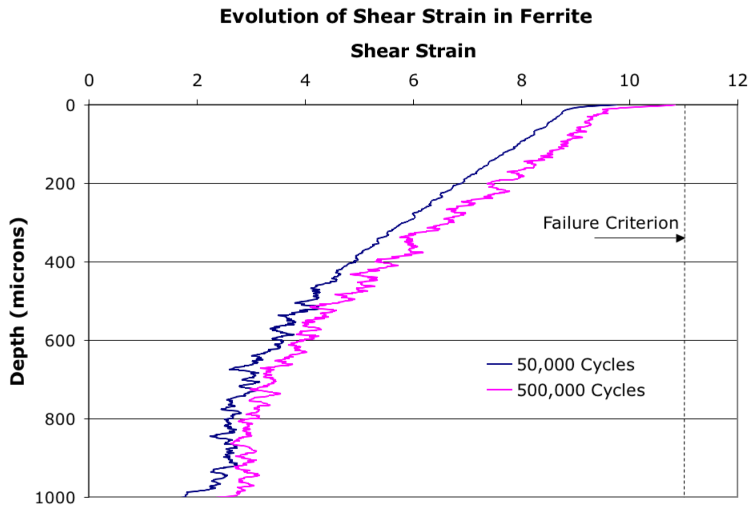

Figure 8: Average accumulated shear strain in the pro-eutectoid ferrite part of the simulated microstructure with a 0.6mm-thick decarburised layer: profile with depth after 50,000 and 500,000 cycles. (The decarburised layer is completely worn away by 500,000 cycles.) The critical shear strain for failure is 11; this is reached only at the surface.

when on average the material at that depth has not reached failure, it is useful to consider the percentage of failure at a particular depth. A higher proportion of failure at a depth indicates a higher likelihood of a crack initiating to this depth.

The 10% Damage Depth, shown in Figure 9 for a Mark 4 coach with average wheel (P8) profiles at four locations at Hatfield (indicated by their distance in metres from a marker) corresponds to the depth at which 10% or more of the elements have failed. The corresponding wear rates are shown in Figure 10, although wear is accounted for in the depths from the surface shown in the 10% damage depth plot Figure 9. Comparable values for a non-decarburised steel can be judged from the later stages of the decarburised simulations because at these stages the decarburised layer has been removed by wear and the steel behaves normally (greater than approximately 450,000 cycles, judged from Figure 10).

The results for Hatfield locations 1512 and 1621 are very similar (although pressure and traction are different, the product μP_0 - related to energy input to the contact $T\gamma$ - is very similar: 456 and 460MPa respectively). For Location 1530, the wear rate is lower and, since the decarburised layer lasts longer, the decay of the 10% Damage Depth is slower. For Location 1650, the pressure is significantly lower than the other three cases, and the traction coefficient also; at this location the wear rate is steady at 0.4nm/cycle and the 10% Damage Depth is negligible. Location 1650 produces results very close to the non-decarburised steel present later in the simulations at the other positions investigated.

For the three locations with the more severe loading conditions (1512, 1530 and 1621), the decarburised layer causes a peak of 340-380 microns in the 10%

Damage Depth after 50,000 cycles. This represents a high probability of crack initiation to that depth at these locations. The comparable depth for a non-decarburised steel, judged from the behaviour late in the simulation after the decarburisation has been worn off would be a 10% damage depth of $5 - 10\mu$m with a high probability of cracks existing to this depth. This shows that the decarburisation has led to around a thirty times increase in the size of cracks which may initiate by ratchetting plasticity accumulation, prior to the removal of the decarburised layer by wear.

Note: Only the top 1mm of the rail is simulated; increasing the depth of simulation may alter the results slightly.

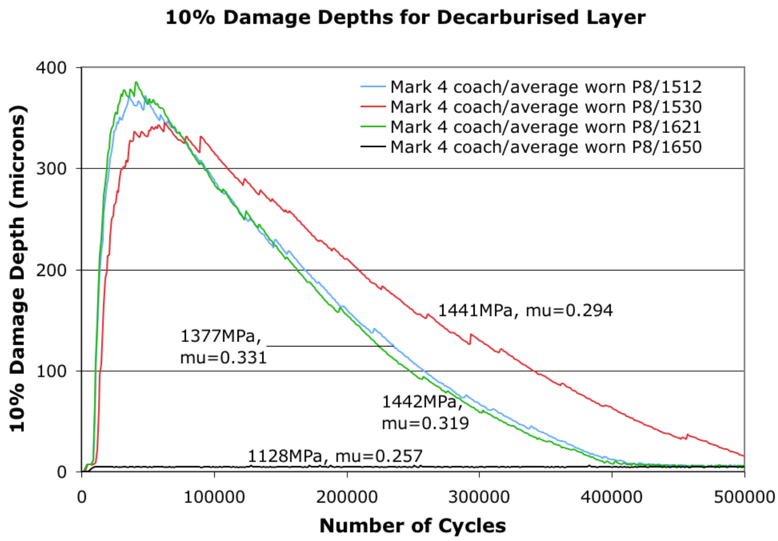

Figure 9: The 10% Damage Depth, for a Mark 4 coach with average wheel (P8) profiles at four locations at Hatfield (1512, 1530, 1621 and 1650 metres from a marker). The 10% damage depth corresponds to the depth at which 10% or more of the elements have failed. "mu" is the surface friction coefficient.

2.4 Development of longer cracks from plastic damage

To access the significance of the cracks initiated in the decarburised layer, a series of 2.5d model runs were undertaken to predict the further growth of the cracks in the decarburised layer. A crack growth law for a decarburised material is not available, so the calculations have used the standard crack growth law for normal grade rail steel, and the results should be treated with caution. No residual stresses were considered in this stage of the modelling.

When wear of the surface is considered (this is truncating cracks, giving a net crack growth rate below that predicted when growth at the crack tip is considered alone) it was found that none of the cracks which developed in the decarburised layer were predicted to grow sufficiently fast to develop into large cracks. For the cases modelled the rapid wear of the decarburised layer is sufficient to prevent large cracks developing. Position 1530 was closest to developing a crack sufficiently large to "overtake" the wear of the material.

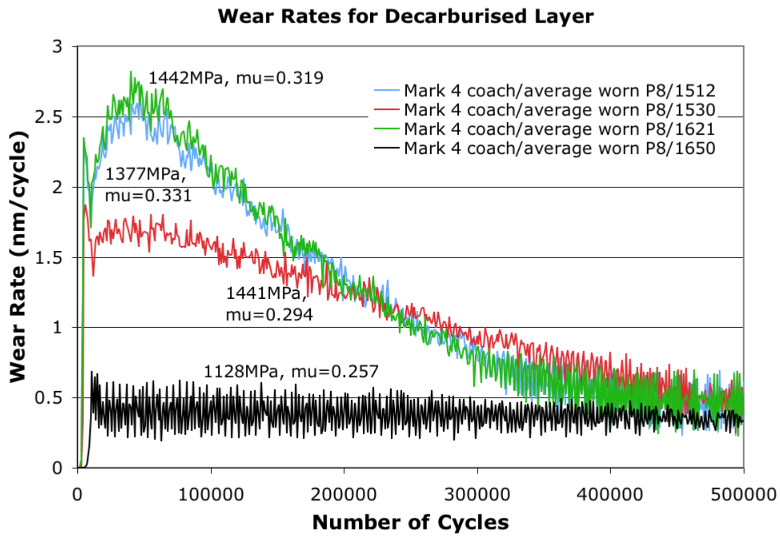

Figure 10: Wear rates for the four vehicle cases in Figure 9.

Further modelling would be required to determine if the cracks initiated in the decarburised layer would go on to grow into large cracks under a wider range of conditions. For example, crack growth would be accelerated, and the size of crack required for sustained growth would be reduced if the surface traction levels were to be increased (i.e. very dry conditions). However, such conditions would also be likely to increase wear, which would itself influence the net crack growth rate.

2.5 Conclusions

The Dynarat "brick" model has been used to simulate a decarburised layer, calibrated using data from twin-disc tests by Carroll and Beynon [10] and Garnham et al. [11]. In the simulation, the decarburised microstructure was represented by a hexagonal pattern of "pearlite" grains with (pro-eutectoid) ferrite grain boundaries, where the thickness of the grain boundaries increased towards the surface. The total thickness of the decarburised layer was 0.6mm.

For the conditions modelled, the wear rate predicted for a rail with a decarburised layer is significantly higher (peaking at 2.5nm/cycle after 50,000 wheel passes) than for a rail without a decarburised layer (a steady wear rate of 0.5nm/cycle). As the decarburised layer is worn away, the wear rate drops to the wear rate for a rail without a decarburised layer.

Comparison of wheel-rail contacts for a Mark 4 coach with average worn (P8) wheels at four locations along the Hatfield curve shows that this wear behaviour occurs only for more severe contact cases (i.e. contact pressure 1377-1442MPa, friction coefficient 0.29-0.33). For more moderate contacts the wear rate is steady and low, similar to the behaviour for rails without a decarburised layer.

The presence of a decarburised layer under the more severe contact conditions modelled is predicted to cause a peak of $340 - 380\mu$m in the depth to which cracks may initiate. The comparable depth for a non-decarburised steel was found to be $5 - 10\mu$m indicating that the decarburisation has led to around a thirty times increase in the size of cracks which may initiate by ratchetting plasticity accumulation, prior to the removal of the decarburised layer by wear.

The decarburised layer is predicted to wear rapidly for the specific conditions modelled. A limited set of crack growth modelling cases shows that the initiated cracks will be worn out before they become established as long cracks driven by contact and residual stresses. However, further modelling would be required to determine the longer term influence of a decarburised layer, beyond the rapid crack initiation period over a wider range of conditions. Influences on the overall effect will include the rapid increase in rail-wheel profile conformity and consequent contact pressure drop brought about by wear of the decarburised surface. The current simulations show that a low contact pressure produces approximately the same depth of damage and crack initiation for a decarburised surface as for a non-decarburised surface. In addition, because of contact size scaling relative to the decarburised layer thickness, twin disc simulation of crack growth in a decarburised surface may produce results different from those for a full-size rail-wheel contact.

3 Validation of 2.5d crack growth model with a 3d crack model

3.1 Introduction to 2.5d model

The majority of crack growth predictions made in work conducted previously [1, 2, 3, 4, 5, 6] were based on a hybrid two and three dimensional model termed the "2.5d" model. This combines underlying two dimensional crack growth solutions with a three dimensional stress field from the rail-wheel contact, acting on a semi-circular crack. During the previous work residual stress in the vertical and longitudinal rail directions were added to this model.

To increase confidence in the 2.5d model, comparisons have been made with alternative fully three dimensional models. This has taken place in three stages: first, comparison with published data from alternative models with no residual stress considered, second, comparison with a three-dimensional model produced in the Beasy boundary element package, again with no residual stress present. The third stage was the comparison of the 2.5d model with boundary element results from a fully three dimensional model including residual stress. While models in the literature are suitable for cases without residual stress included in the model, only with the boundary element model was it possible to produce results for a fully three dimensional model including residual stress.

3.2 Background

An important aspect of the crack growth modelling previously conducted was the use a hybrid model combining both two and three dimensional features. The model was based on Green's functions [12] for the conversion of the stress present in a body into a stress intensity factor for prediction of crack growth rate.

Figure 11 indicates visually how Green's functions are applied in calculating a stress intensity factor.

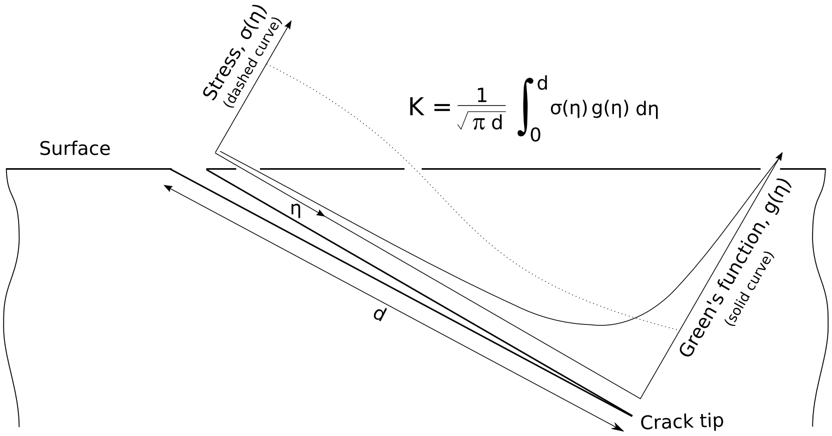

Figure 11: Schematic representation of a surface crack showing stress intensity factor (K) calculation by combining the stress distribution and Green's function along the line of the crack. Separate Green's functions are needed to calculate the effect of stress normal and parallel to the crack on the mode I and II stress intensity factors. Stress distributions are those in the uncracked body.

The Green's functions developed by Rooke [12] were first applied to calculation of stress intensity factors for rolling contact fatigue cracks in the models developed by Fletcher and Beynon (F&B) [13, 14] for modelling cracks found in twin disc contact simulations [15]. The Green's functions currently available for shallow angle surface breaking cracks of the type found in rolling contact fatigue are restricted to a two dimensional representation of the crack and load. In this representation a line contact passes over an infinitely wide crack (Figure 12 shows a cross-section of such a crack), so although the shallow angle of the crack is correctly represented, there are significant differences from the cracks and loads present in rail-wheel contact.

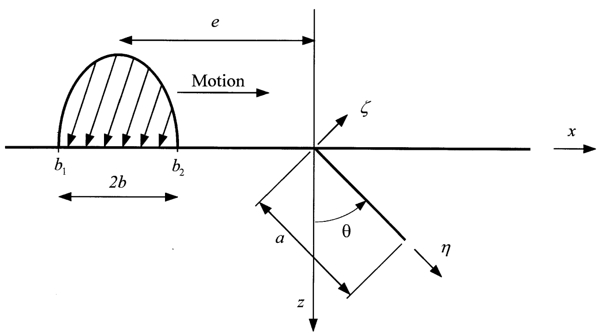

Figure 12: Schematic of a contact crossing an inclined crack below a rail surface.

The models developed by F&B addressed the problem of converting results for an infinitely wide crack into predictions for a more realistic semi-circular shape crack by using a geometry factor for the crack, a standard fracture mechanics approach to the issue. This was generated by taking the ratio of stress intensity factors for the semi-circular and infinitely wide cracks from standard results available for these crack configurations in pure tension and pure bending. At this time the models were primarily for application in understanding crack growth in twin disc contact simulations, so the configuration of a line contact passing over a semi-circular crack was a good representation of the physical simulation.

For application of the F&B model to real rail-wheel contact further development has been undertaken to account for the three-dimensional nature of the contact between rail and wheel, which is much closer to an elliptical rather than a line contact. One approach would be the development of further Green's functions for three dimensional cracks, but this requires considerable work, and was beyond the scope of the project, therefore a hybrid 2d-3d approach was taken.

Validation of stress intensity factors for semi-circular cracks was conducted against published data for this crack shape beneath line contacts at the time the model was published [13, 14]. In this section validation of the developments in the model to include 3d rather than 2d contacts is presented, using two approaches. First, the output of the 2.5d model is compared with data published by Kaneta and Murakami (K&M) [16] for three-dimensional circular contacts passing over three dimensional cracks. Second, the output of the 2.5d model is compared to a fully three dimensional model developed in the Beasy boundary element modelling software.

3.2.1 Detail of elliptical contact patch implementation

The Green's functions developed by Rooke et al. [12] which underlie the stress intensity factor calculation method developed by F&B are for two-dimensional cracks. However, their use depends only on the stress present along the centre line of the crack, which for a two-dimensional crack is uniform across (infinite) the width of the crack, and this stress can be generated by any arbitrary surface loading on the boundary of the cracked body. Previously, a two-dimensional contact loading was used in the stress intensity factor calculation, but in the newly developed cases this is replaced by a Hertzian elliptical contact patch. For a contact running centrally over a crack it is assumed that the stress on the plane below the centreline of the contact patch controls crack growth[1]. This is the plane on which the highest stresses will lie for a contact under normal pressure and tangential traction in the direction of motion across the crack. In addition, any hunting or lateral wandering of the contact between wheels will ensure that a wide area of the imagined two dimensional crack is subjected to these high levels of stress. To reflect the combination of two and three-dimensional components, the model has become known as the 2.5d model [17], and this is shown schematically in Figure 13.

An elliptical contact patch produces stresses which diminish more rapidly with depth into the material than does a line contact [18], and this difference is successfully captured by combining the three-dimensional contact patch with

[1] In rail-wheel contact successive wheels may not follow each other over exactly the same path. Different parts of the crack may therefore be below the contact centreline and subject to the highest levels of stress. The method presented here is for a central contact position only.

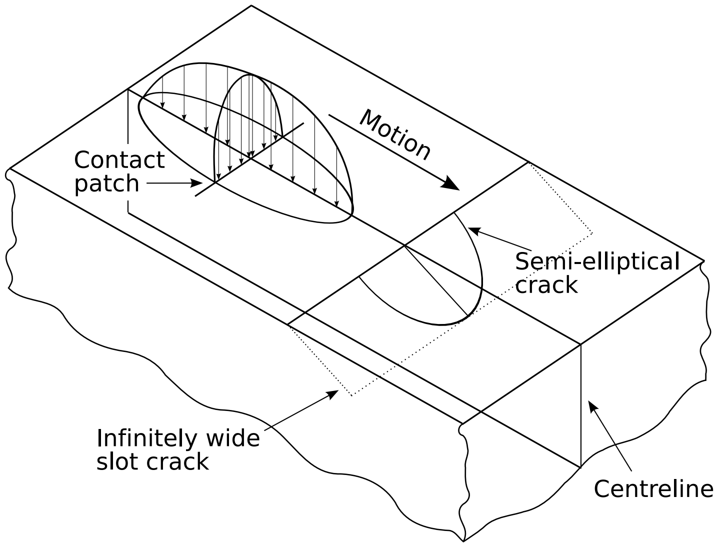

Figure 13: Schematic representation of the 2.5d model. Stresses on the centreline below a three-dimensional elliptical contact are used to predict crack growth using Green's functions for an infinitely wide "slot" type crack. In reality, any hunting or lateral wandering of the contact between wheels will ensure that a wide area of the imagined two dimensional crack is subjected to these high levels of stress. A geometry factor is used to translate the results to a stress intensity factor for the deepest point of a semi-elliptical crack.

the two dimensional Green's functions.

Stress diminishes with increasing depth into the material, but also falls with increasing lateral distance either side of an elliptical contact. With the exception of gross offset of the contact away from the crack (such as may be produced by rail grinding) it is not possible to capture this reduction, or its effect on crack locking and closure across the crack faces, because of the underlying two-dimensional nature of the method. Similarly, the variation of stress intensity factor with position around the crack front of a three dimensional crack cannot be captured. Stress intensity factors are based on the locking and closure of the crack below the centreline of the contact. This represents the deepest and therefore most critical point of the crack front for determining growth.

Results are given below for the comparison between output of the 2.5d model and previously published data by Kaneta and Murakami (K&M) [16]. The conditions modelled were restricted to those of the published data, and consisted of a circular contact passing over a semi-circular crack.

3.3 Boundary element model development

The boundary element modelling software Beasy [19] was used to build a three dimensional representation of 400mm of rail, including the head, web and foot. An overview is shown in Figure 14. Boundary element rather than finite element software was chosen because it has greatly reduced computing requirements when studying regions of material in which there are very high stress gradients, such as exist ahead of cracks. This is because the problem is treated mathematically as a series of integrals over the boundary surface of the rail, rather than through its volume. The technique includes the assumption of elastic behaviour within the rail, and while this would be unsatisfactory for very small cracks (hundred microns scale) lying in severely plastically deformed material very close to the rail surface, it is reasonable for longer cracks reaching deeper into the rail head.

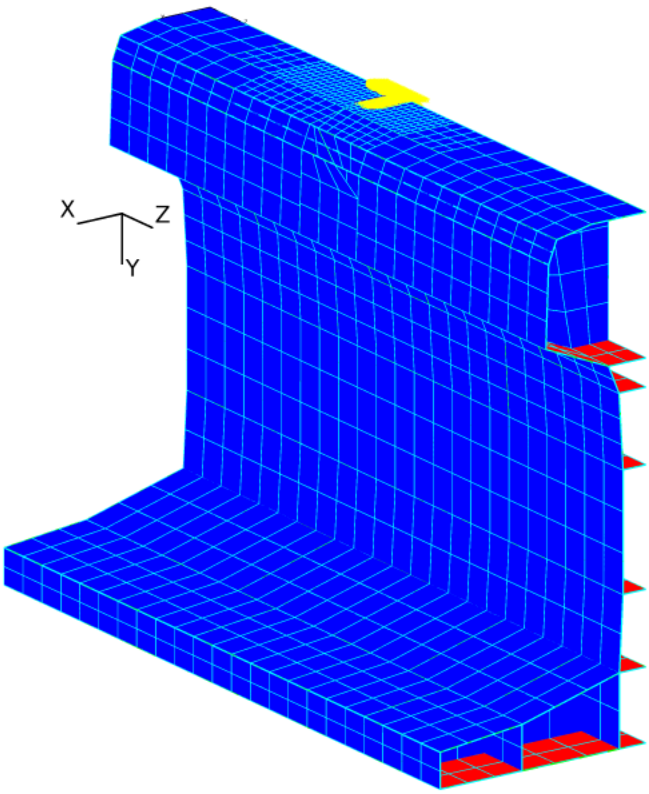

Figure 14: Overview of the Beasy boundary element model. Symmetry of the rail and central positioning of the wheel contact allowed a half rail model to be created, greatly reducing the computing requirements. Divisions inside the model show "zoning" of the model into smaller regions of near cubic shape, which increased solution speed.

Contact pressure was applied in the boundary element model to duplicate the Hertzian contact applied in the 2.5d model. When using numerical techniques such as boundary elements it is possible to create a more accurate representation of the contact, rather than simply duplicating the Hertzian contact. However, the purpose of the Beasy model was to validate the stress intensity predictions in the three dimensional body, not to validate the Hertzian contact assumptions, so it was important to retain the Hertzian contact geometry. The wheel load was applied using a closely spaced array of point loads at the surface of the rail. Examination of the internal stress in the rail prior to inserting the crack showed that this approach gave stresses very close to those of an ideal Hertzian contact.

Longitudinal traction forces were applied in the same way, and similarly checked.

3.4 Conditions modelled

The rail was constrained in the vertical direction at its foot along the entire length (i.e. no rail bending could occur) and defined as infinite in the longitudinal direction. The wheel contact was placed in the centre of the rail crown, and a symmetry condition used to prevent lateral motion. The cracks modelled were of 5 and 10mm radius, and were inclined at 30° below the rail surface. The model was of a shear crack growth mechanism with contributions from both mode I and II stress intensities, and included friction between the crack faces. Table 1 shows the friction conditions modelled, both on the rail surface, and on the crack faces.

Contact Pressure MPa	Crack radius mm	Surface friction coefficient	Crack face friction coefficients
1750	5	0.15	0.05, 0.15, 0.30, 0.45
1750	5	0.30	0.15, 0.30
1750	5	0.45	0.05, 0.15, 0.30, 0.45
1750	10	0.30	0.05, 0.15, 0.30, 0.45

Table 1: Conditions examined for 3d Beasy modelling runs without residual stress. In all cases cracks were at 30° below the rail surface.

3.5 Results

3.5.1 Murakami and Kaneta

The stress intensity factors predicted by the 2.5d model are presented in the non-dimensional form used by K&M to allow easy comparison between these reference cases and the current results. Equation 1 shows the relationship between dimensional (K) and non-dimensional (F) stress intensity factor, contact pressure (p_0) and h, where h is the crack radius.

$$K = Fp_0\sqrt{\pi h} \tag{1}$$

Stress intensities are presented using the shear mode stress intensity factor (K_τ) defined by Equation 2 [20], which combines mode I (K_I) and mode II (K_{II}) stress intensities at an angle θ ahead of the crack and is solved to find the largest shear mode stress intensity present.

$$K_\tau = \frac{1}{2}\cos\frac{\theta}{2}[K_I \sin\theta + K_{II}(3\cos\theta - 1)] \tag{2}$$

Graphs of the stress intensity factors show the normalised position of the contact patch relative to an origin at the crack mouth. In each case the position is normalised by the contact radius.

Figure 15a shows the crack configuration used by K&M [16] to model a circular contact patch crossing the centre line of a semi-circular crack. Figure 16 shows the stress intensity factor results for this case, together with results from the 2.5d model for the same contact size and shape. The crack modelled is a short crack, with a radius of 0.1 times the contact patch radius, lying at 45° below the surface. For a rail-wheel contact this would give a crack radius of approximately 0.5 to 1mm.

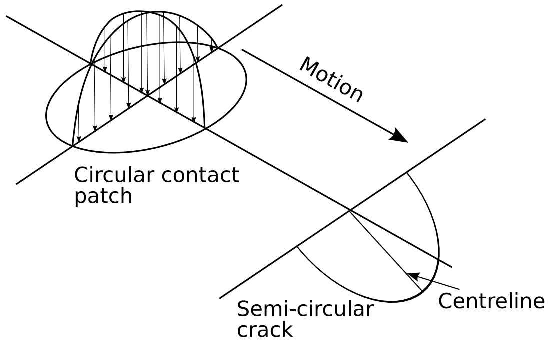

Figure 15: The three dimensional contact patch approaching an inclined semi-circular surface breaking crack, modelled by Kaneta and Murakami [16, 21].

The results shown in Figure 16 indicate good agreement between the K&M reference data and the output of the 2.5d model. The agreement at low values of surface traction is particularly good. At higher surface traction levels (the highest examined was 0.3) the 2.5d model indicates a stress intensity factor range of around 80% that predicted by K&M [16]. This deviation is almost identical to that observed for the previously published line contact versions of the Green's function based 2d model [13, 14].

Most importantly, the trends predicted by both the K&M data and the 2.5d model are identical, i.e. both models predict that stress intensity factor values (and hence crack growth rates) fall as the crack face friction coefficient increases, and rise with increasing surface traction.

3.5.2 Beasy three-dimensional model

Figures 17 and 18 show results similar to those discussed above, but with the three dimensional case generated using the Beasy boundary element model, together with comparable runs using the 2.5d model. In these cases the dimensional rather than non-dimensional stress intensity factors have been plotted, but the comparison between the cases is unaffected by this. It is already known from the comparison of 2.5d modelling output with the work of K&M [16] that the 2.5d model performs well, so the comparison here is most valuable in understanding the performance of the Beasy model.

Crack growth rate is determined by the range of stress intensity factor experienced during the passage of the wheel. In comparing the Beasy and 2.5d output it is therefore the peaks and troughs and the difference in their positions relative to the contact that are most important. From Figures 17 and 18 it can be seen that the form of mode I (opening) and mode II (shearing) results is very similar for the two modelling methods, with results for mode II being particularly good. This indicates that the Beasy model is working well, and particularly since the mode II results are good, that the presence of friction between the crack faces has been captured well.

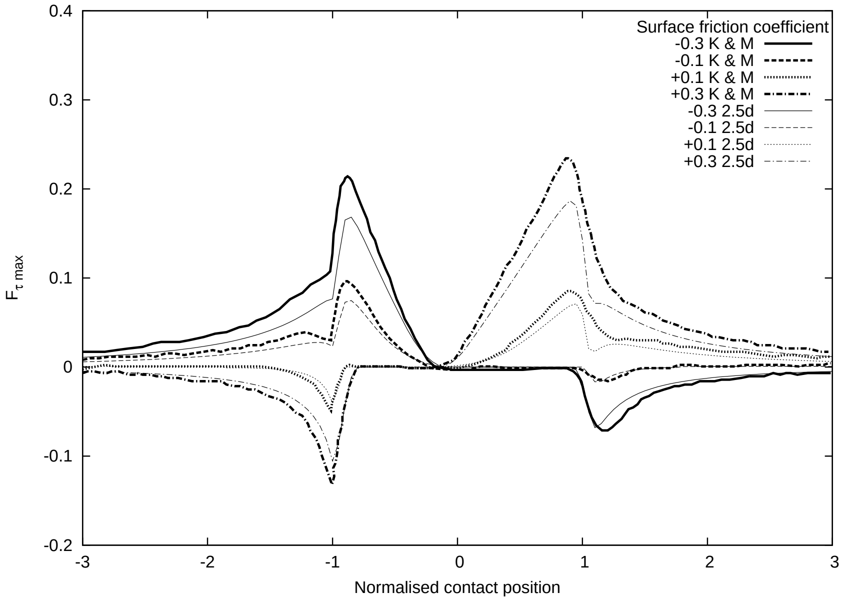

(a)

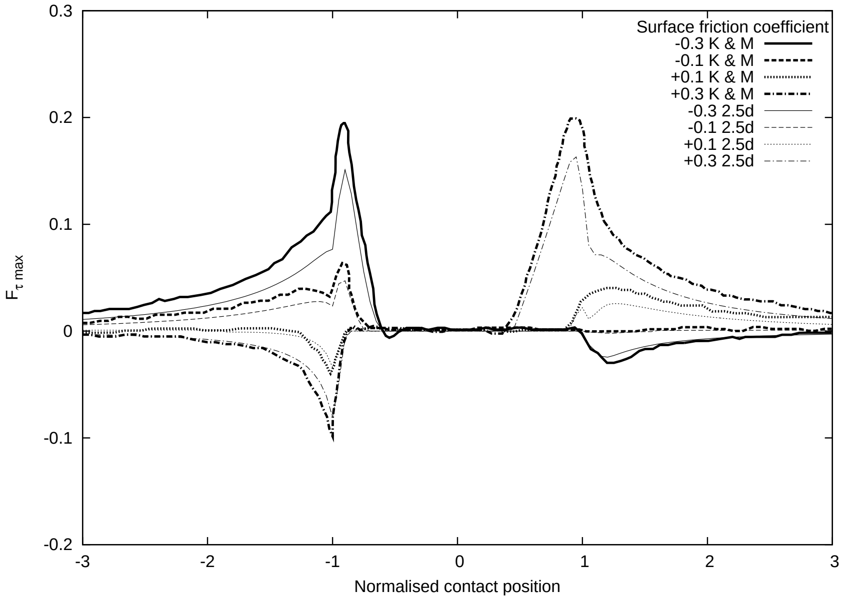

(b)

Figure 16: Normalised stress intensity factor results for shear growth of a semi-circular crack beneath a circular contact patch. Results from Kaneta et al. (K&M) are shown together with results from the 2.5d model. The key indicates the surface traction coefficient applied in each case. (a) Crack face friction coefficient of 0.2. (b) Crack face friction coefficient of 0.5.

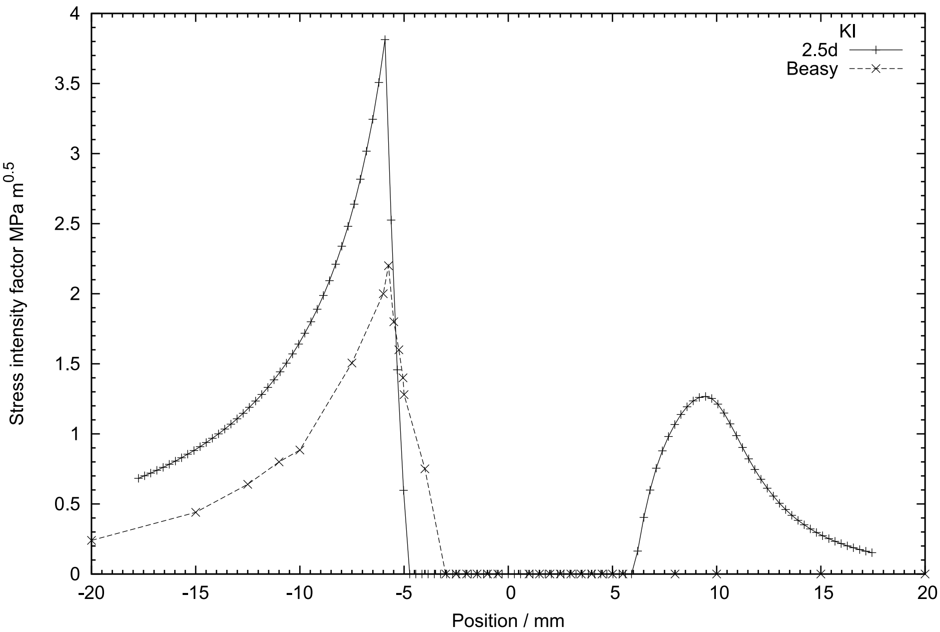

(a)

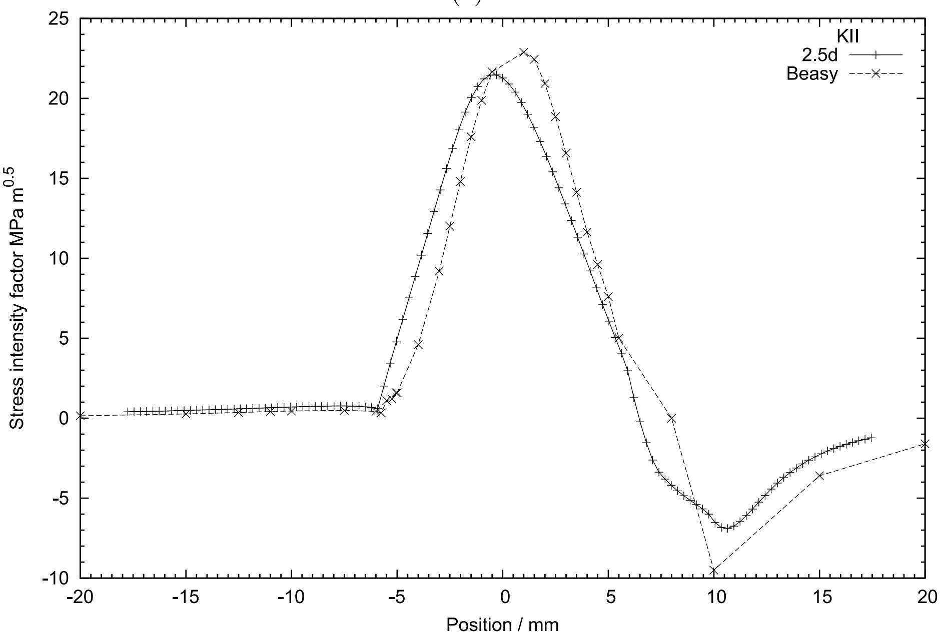

(b)

Figure 17: Stress intensity factor variation with contact position for the Beasy boundary element model (dotted lines) with corresponding 2.5d model runs (solid lines). Crack radius 5mm, Hertzian contact pressure 1750MPa, surface and crack face friction coefficient 0.15. The crack lies to the positive side of the position axis, with its mouth at the origin. (a) Mode I (opening) stress intensity factors. (b) Mode II (shearing) stress intensity factors.

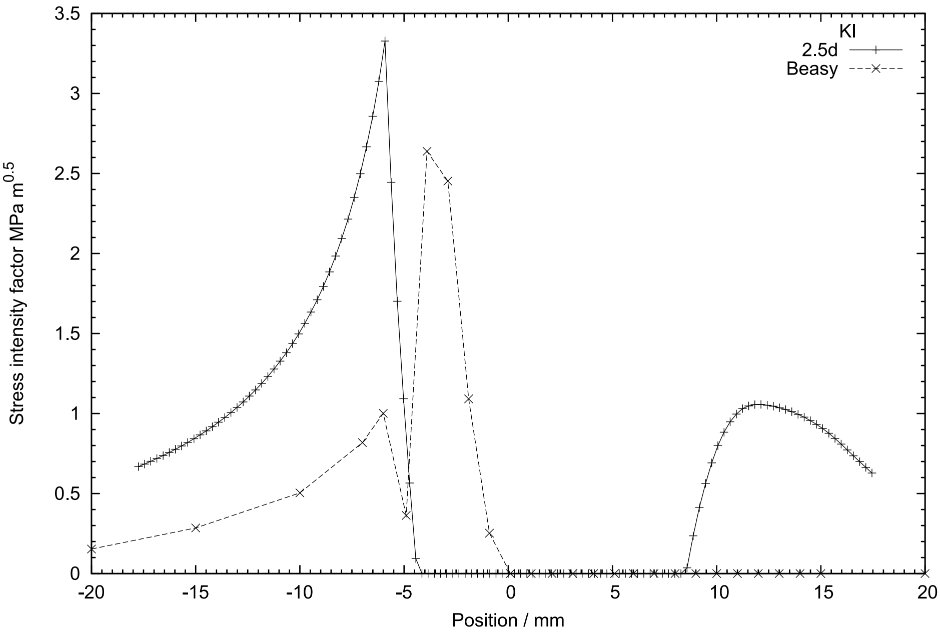

(a)

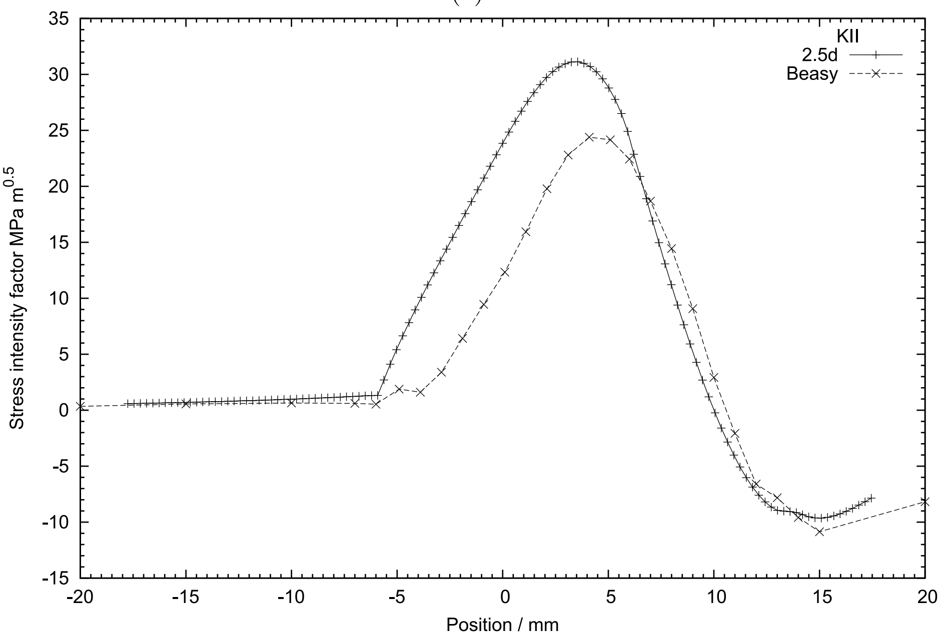

(b)

Figure 18: Stress intensity factor variation with contact position for the Beasy boundary element model (dotted lines) with corresponding 2.5d model runs (solid lines). Crack radius 10mm, Hertzian contact pressure 1750MPa, surface friction coefficient 0.30, crack face friction coefficient 0.05. The crack lies to the positive side of the position axis, with its mouth at the origin. (a) Mode I (opening) stress intensity factors. (b) Mode II (shearing) stress intensity factors.

Results for mode I differ at the peak in stress intensity factor which is produced just as the contact begins to move over the crack (left side of mode I graphs) with this peak being lower in the Beasy modelling output. In addition, the second peak (right side of mode I graphs) predicted by the 2.5d model is absent from the Beasy results, although since this is the lower of the peaks it is not considered in crack growth rate determination.

It is thought that the differences in mode I results are due to the use of an array of individual point loads to apply the Hertzian pressure to the rail surface in the Beasy model, whereas a continuous pressure distribution is used in the 2.5d model. It is inevitable that however many point loads are used, very close to the rail surface the pressure distribution produced will not be as smooth as a mathematically continuous distribution. The peak mode I stress intensity factor occurs at the moment the contact pressure just begins to cross the crack, and this will take place differently for a continuous pressure distribution, and for a array of point loads. This difference is unavoidable when representing the smooth Hertzian pressure distribution with a less smooth array of points loads in the Beasy model. Since the current model focuses on shear mode crack growth, these differences in mode I have a much smaller impact on crack growth predictions than would a similar difference in mode II peaks.

4 A three dimensional crack growth model including residual stress

The Beasy model described above was further developed to subject the crack to residual stresses in addition to contact loading. Other features of the model such as the choice of a Hertzian contact load remained unchanged, allowing comparison with earlier results so as to reveal the effect of residual stress.

4.1 Application of residual stress

Residual stresses[2] were applied following consultation with Beasy staff on the most appropriate way to apply internal forces to the model. i.e. forces within the rail which remain present even when the external wheel load is removed. To produce the residual stress an array of internal point loads was defined on inclined planes either side of the crack. The point loads were distributed so as to produce the required vertical and longitudinal residual stress distributions along the plane of the crack. Figure 19 shows the distribution of these points either side of the crack. Transverse residual stresses were not modelled, since they had not been included in the 2.5d model, although they could be added to the Beasy model in the future. The spacing between the point loads was small relative to their distance from the crack, ensuring a smooth residual stress distribution at the crack.

[2]It was originally planned that the modelling work for validating the 2.5d model against the three dimensional model would use residual stress data obtained by measurements on a section of MHT rail from the Hatfield site. However, the data could not be obtained during this project. Use of alternative data does not affect the validation, since validation is independent of the residual stress profiles used providing that the same profiles are used in both modelling approaches.

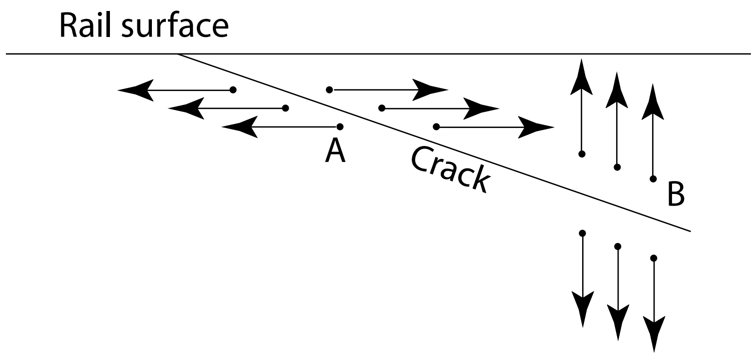

Figure 19: Schematic representation of residual stresses application using internal point loads on planes either side of the crack. Both longitudinal (A) and vertical (B) residual stresses were applied in this way along the full length of the crack (points are only shown over part of the crack length for clarity).

A check on the stress distribution produced by the point loads used to represent the residual stress showed slight deviation (15-20%) from the intended stress profile, which had been applied in previous modelling work [1]. Further 2.5d modelling runs were therefore conducted using the residual stress distribution actually achieved in Beasy. This ensured that crack growth in the 2.5d and 3d Beasy runs was modelled for the same driving stress, and that imperfections in residual stress application within Beasy did not affect the comparison of the two modelling methods.

4.2 Results

Table 2 shows the conditions modelled using Beasy for cases including residual stress, and some typical results are shown in Figures 21 and 22. The full set of results in included in the Appendix.

Contact Pressure MPa	Crack radius mm	Surface friction coefficient	Crack face friction coefficients
1750	5	0.15	0.05, 0.15, 0.30, 0.45
1750	5	0.30	0.05, 0.15, 0.30, 0.45
1750	5	0.45	0.05, 0.15, 0.30, 0.45
1750	10	0.00	0.05, 0.15, 0.30, 0.45
1750	10	0.15	0.05, 0.15, 0.30, 0.45
1750	10	0.30	0.05, 0.15, 0.30, 0.45
1750	10	0.45	0.05, 0.15, 0.30, 0.45

Table 2: Conditions examined for 3d Beasy modelling runs including residual stress

Mode I stress intensity factor was predicted to be zero for all cases modelled using Beasy, just as mode I results were lower than found with the 2.5d model in cases without residual stress applied. For cases with residual stress the mode

I results predicted by the 2.5d model were of low magnitude, and in most cases below the fatigue threshold of $4MPa\sqrt{m}$ (Figure 20).

The direction of crack branching is dependant on the ratio of mode I to mode II stress intensity factor, as discussed in [4] and summarised by Equations 2 and 3. The direction of branch crack growth (θ_τ) can be found by taking the root of Equation (3) relative to the initial crack growth direction which gives the maximum value of the equivalent shear mode stress intensity factor K_τ .

$$\tan^3\frac{\theta_\tau}{2} - \frac{1}{\gamma}\tan^2\frac{\theta_\tau}{2} - \frac{7}{2}\tan\frac{\theta_\tau}{2} + \frac{1}{2\gamma} = 0, \gamma = \frac{K_{II}}{K_I} \quad (3)$$

A zero mode II stress intensity factor implies that crack growth will take place without branching, i.e. for a 30° crack, growth will continue at 30°. However, experimental work [22] has identified that in practise a mode I stress in addition to the mode II is required to prevent branching. Since short cracks in the rail are known to grow with an approximately constant inclination to the rail surface, this suggests that the prediction of the 2.5d model may be more realistic than the zero mode I prediction of Beasy.

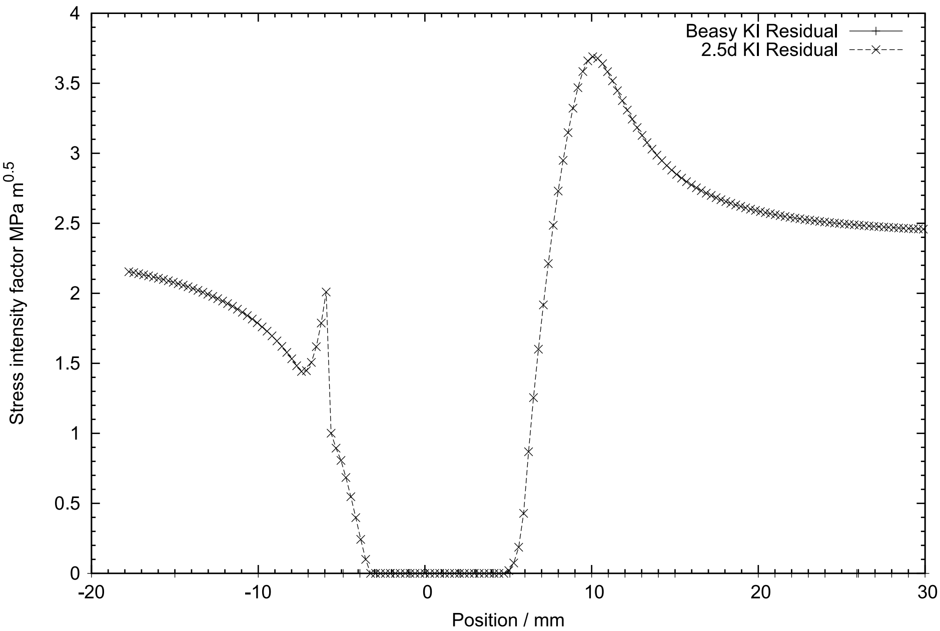

(a)

Figure 20: Mode I stress intensity factor results from the 2.5d model, including residual stress. The values are low, and alone (i.e. without combination with mode II stress intensity factors) fall below the fatigue threshold of $4MPa\sqrt{m}$. Note that there remains a positive stress intensity factor present even at the extremes of contact position, when the wheel load is well away from the crack. This is driven by the crack opening effect of the residual stress, present even when the contact has moved away.

Because of the zero predictions for mode I stress intensity factor predictions from Beasy, the comparison between the 2.5d modelling results and those from

Beasy with residual stress included is made solely using the mode II stress intensity factors. From Figures 21 and 22 it can be seen that, as in the case without residual stress applied, the form of the curves for the 2.5d and Beasy 3d models is very similar. Also similar is the stress intensity factor range during the passage of the contact. This range is summarised in Table 3 for the results shown in Figures 21 and 22.

Crack radius mm	Surface friction coef	Crack face friction coef	SIF range 2.5d $MPa\sqrt{m}$	SIF range Beasy $MPa\sqrt{m}$	Beasy SIF range as a percentage of 2.5d model prediction
5	0.15	0.15	30.0	34.6	115%
5	0.30	0.30	21.8	26.2	120%
10	0.15	0.15	34.6	38.4	111%
10	0.30	0.30	23.4	32.6	139%

Table 3: Mode II stress intensity factor (SIF) summary for runs with residual stress.

From Table 3 it can be seen that the trends in stress intensity factor range predicted are the same for both models, with the higher friction case giving lower mode II stress intensity factor range at both crack sizes modelled. Differences in stress intensity factor range between the two models are greatest under higher friction conditions.

Results for both models show that the crack remain under stress even when the contact has moved away from the crack, indicated by the negative values of stress intensity at the extremes of contact position in Figures 21 and 22. This shows that the residual stress biases the crack faces to slide over one another relative to their stress free position. The models without residual stress present show a zero stress intensity factor at these positions (Figure 16). This bias is stronger in the 3d Beasy model than in the 2.5d model, and although the form of the curves is similar, the Beasy results lie $10 - 15MPa\sqrt{m}$ below the 2.5d results during much of the passage of the contact.

Initially it was thought that the difference in bias between the 2.5d and Beasy model was the result of the true three dimensional nature of the railhead modelled in Beasy, relative to the half-space assumption of the contact models underlying the 2.5d model. In the 2.5d model the crack never reaches or even approaches the "edge" of the rail head. In the Beasy model the crack can do this, and as it does so the stress affecting its growth diverges from those present in the half-space. However, testing models with artificially large rail head cross-sections in Beasy showed that the stress intensity factor results were unaffected by changing the rail head size. Further research is required to fully understand the difference between the two models in this case.

From the comparison of the output from the 2.5d model with fully three dimensional Beasy modelling output it can be seen that there is reasonable agreement between the two methods, particularly when considering the highly complex conditions to which the crack is subjected during the passage of a wheel contact. Further research is required to understand the differences, but it should also be remembered that perfect agreement was not reached when comparing Beasy modelling output with results from models by Murakami and Kaneta [16] for cases without residual stress applied.

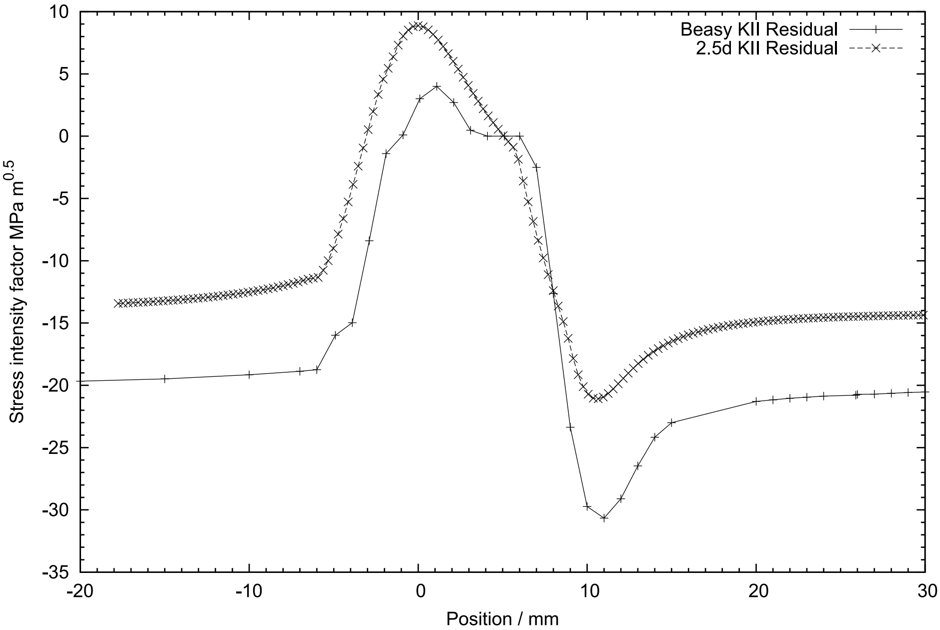

(a)

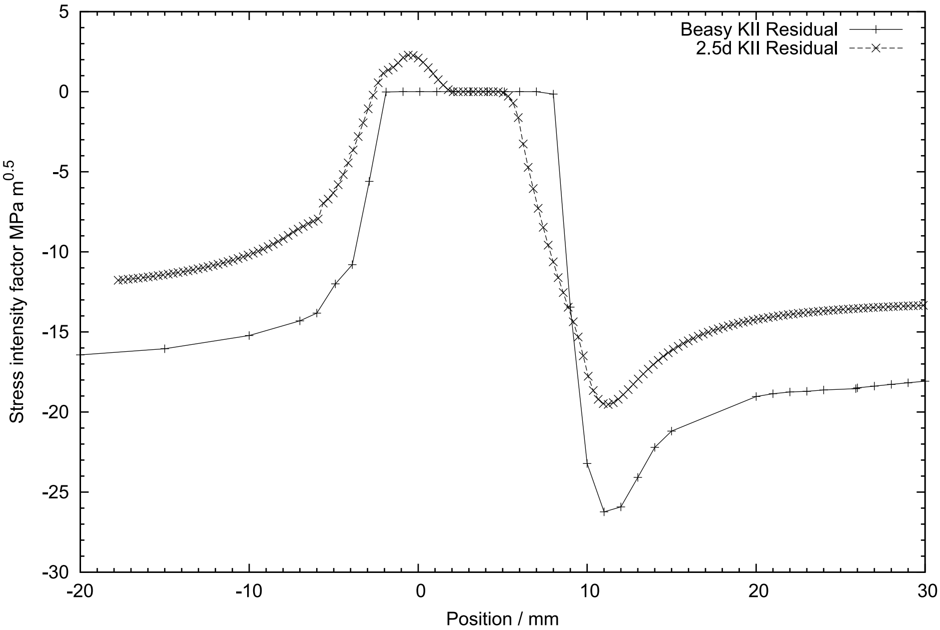

(b)

Figure 21: Mode II Beasy and comparable 2.5d modelling results for a 5mm radius crack. (a) Surface and crack face friction coefficient of 0.15. (b) Surface and crack face friction coefficient of 0.30.

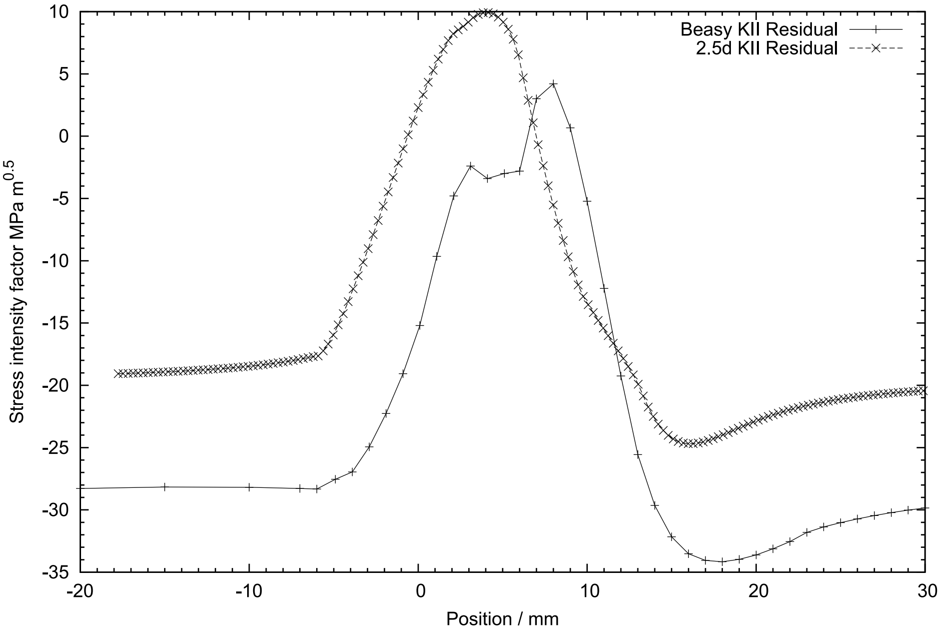

(a)

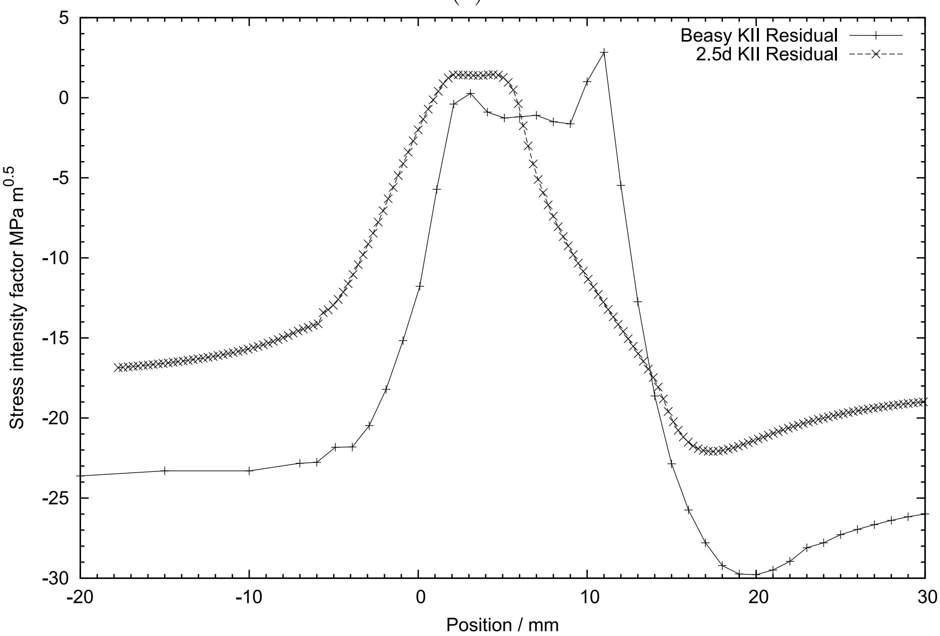

(b)

Figure 22: Mode II Beasy and comparable 2.5d modelling results for a 10mm radius crack. (a) Surface and crack face friction coefficient of 0.15. (b) Surface and crack face friction coefficient of 0.30.

The agreement found between the Beasy and 2.5d models indicates that trends in crack growth predicted using the 2.5d model will be very close to those which could be predicted by further runs of the fully three dimensional Beasy model. The important advantage of the 2.5d model is its fast run speed, which allows a wide variety of conditions to be examined. Both models predict that cracks of 5mm and 10mm radius will grow straight ahead, without branching. Only at longer crack lengths (larger than 15-20mm radius) [4] did the 2.5d model predict branching to take place for cases including residual stress.

5 Conclusions

5.1 Rail decarburisation and crack initiation

The Dynarat “brick” model has been used to simulate a decarburised layer using a hexagonal pattern of “pearlite” grains with (pro-eutectoid) ferrite grain boundaries, where the thickness of the grain boundaries increased towards the surface.

Under the conditions modelled, the wear rate predicted for a rail with a decarburised layer is significantly higher than for a rail without a decarburised layer, but as the decarburised layer is worn away, the wear rate drops to the wear rate for a rail without a decarburised layer.

The presence of a decarburised layer is predicted to cause a peak of up to $340 - 380\mu$m in the depth to which cracks may initiate, for the conditions simulated. The comparable depth for a non-decarburised steel was found to be $5 - 10\mu$m, indicating that the decarburisation has led to around a thirty times increase in the size of cracks which may initiate by ratchetting plasticity accumulation, prior to the removal of the decarburised layer by wear.

For the contact conditions considered, the decarburised layer is predicted to wear rapidly. A limited set of crack growth modelling cases shows that the initiated cracks will be worn out before they become established as long cracks driven by contact and residual stresses. However, further modelling would be required to determine the longer term influence of a decarburised layer, beyond the rapid crack initiation period over a wider range of conditions. Influences on the overall effect will include the rapid increase in rail-wheel profile conformity and consequent contact pressure drop brought about by wear of the decarburised surface. The current simulations show that a low contact pressure produces approximately the same depth of damage and crack initiation for a decarburised surface as for a non-decarburised surface. In addition, because of contact size scaling relative to the decarburised layer thickness, twin disc simulation of crack growth in a decarburised surface may produce results different from those for a full-size rail-wheel contact.

5.2 Long crack growth modelling

To increase confidence in the results produced by the “2.5d” crack growth model three stages of validation using alternative models have been undertaken.

- First, the output of the “2.5d” model without residual stress applied was compared to published data from an alternative model, showing good agreement in the results. The agreement at low values of surface traction is particularly good. At higher surface traction levels (the highest examined was 0.3) the 2.5d model indicates a stress intensity factor range of around 80% that predicted by K&M [16]. This deviation is almost identical to that observed for the previously published line contact versions of the Green's function based 2d model [13, 14].

Most importantly, the trends predicted by both the K&M data and the 2.5d model are identical, i.e. both models predict that stress intensity factor values (and hence crack growth rates) fall as the crack face friction coefficient increases, and rise with increasing surface traction.

- Second, again without residual stress applied, a fully three dimensional boundary element model was created using the Beasy modelling software, and its results compared to those from the 2.5d model. The comparison showed that the form of mode I (opening) and mode II (shearing) results was very similar for the two modelling methods, with results for mode II being particularly good. This indicates that the Beasy model is working well, and particularly since the mode II results are good, that the presence of friction between the crack faces has been captured well.

  It was thought that the differences in mode I results are due to the use of an array of individual point loads to apply the Hertzian pressure to the rail surface in the Beasy model, whereas a continuous pressure distribution is used in the 2.5d model.

- Third, residual stress was added to the Beasy boundary element model, enabling comparison to be made with the 2.5d method including residual stress. The agreement found between the Beasy and 2.5d models indicates that trends in crack growth predicted using the 2.5d model will be very close to those which could be predicted by further runs of the fully three dimensional Beasy model. Both models predict that cracks of 5mm and 10mm radius will grow straight ahead, without branching. However, there were some differences between the models in mode I stress intensity factor results, and in the static values of stress intensity factor present when the wheel contact is remote from the crack. Further research is required to fully understand these differences, although the results of the two independently created models were in generally good agreement considering the complexity of the contact and residual stress regime being modelled.

References

[1] A Kapoor and D I Fletcher. Post Hatfield rolling contact fatigue. The effect of residual stress on contact stress driven crack growth in rail. Literature review. Technical Report WR061106-1, Newcastle University, November 2006.

[2] A Kapoor and D I Fletcher. Post Hatfield rolling contact fatigue. The effect of residual stress on contact stress driven crack growth in rail. Part 1: The model. Technical Report WR061106-2, Newcastle University, November 2006.

[3] A Kapoor and D I Fletcher. Post Hatfield rolling contact fatigue. The effect of residual stress on contact stress driven crack growth in rail. Part 2: Data. Technical Report WR061106-3, Newcastle University, November 2006.

[4] A Kapoor and D I Fletcher. Post Hatfield rolling contact fatigue. The effect of residual stress on contact stress driven crack growth in rail. Part 3: Further Data. Technical Report WR061106-4, Newcastle University, November 2006.

[5] D I Fletcher and A Kapoor. Post Hatfield rolling contact fatigue. The effect of residual stress on contact stress driven crack growth in rail. Combination of bending and contact stesses. Technical Report WR061106-5, Newcastle University, November 2006.

[6] J Hobbs. Modelling of bending stress in rails, HSL Report MM0429, Project JR 31.086 Post Hatfield rolling contact fatigue. Technical report, Health & Safety Laboratory, Broad Lane, Sheffield, S3 7HQ, UK, 2004.

[7] A Kapoor. A re-evaluation of the life to rupture of ductile metals by cyclic plastic strain. *Fatigue and Fracture of Engineering Materials and Structures*, 17:201–219, 1994.

[8] F J Franklin, T Chung, and A Kapoor. Ratcheting and fatigue-led wear in rail-wheel contact. *Fatigue and Fracture of Engineering Materials and Structures*, 26:949–955, 2003.

[9] F J Franklin and A Kapoor. Modelling wear and crack initiation in rails. *Submitted to IMechE Journal of Rail and Rapid Transit*, 2006.

[10] R I Carroll and J H Beynon. Decarburisation and rolling contact fatigue of a rail steel. *Wear*, In Press, 2006.

[11] J E Garnham, F J Franklin, D I Fletcher, A Kapoor, and C L Davis. Predicting the life of steel rails. *Submitted to IMechE Journal of Rail and Rapid Transit*, 2006.

[12] D P Rooke, D B Rayaprolu, and M H Aliabadi. Crack line and edge green's functions for stress intensity factors of inclined edge cracks. *Fatigue and Fracture of Engineering Materials and Structures*, 15(5):441–461, 1992.

[13] D I Fletcher and J H Beynon. A simple method of stress intensity factor calculation for inclined fluid-filled surface-breaking cracks under contact loading. *Proceedings of the Institution of Mechanical Engineering Part J, Journal of Engineering Tribology*, 213:299–304, 1999.

[14] D I Fletcher and J H Beynon. A simple method of stress intensity factor calculation for inclined surface breaking cracks with crack face friction under contact loading. *Proceedings of the Institution of Mechanical Engineering Part J, Journal of Engineering Tribology*, 213:481–486, 1999.

[15] D I Fletcher and J H Beynon. The effect of contact load reduction on the fatigue life of pearlitic rail steel in lubricated rolling-sliding contact. *Fatigue and Fracture of Engineering Materials and Structures*, 23:639–650, 2000.

[16] M Kaneta, M Suetsugu, and Y Murakami. Mechanism of surface crack growth in lubricated rolling/sliding spherical contact. *ASME Journal of Applied Mechanics*, 53:354–360, 1986.

[17] D I Fletcher and A Kapoor. A rapid method of stress intensity factor calculation for semi-elliptical surface breaking cracks under three-dimensional contact loading. *Proceedings of the Institution of Mechanical Engineers, Part F, Journal of Rail and Rapid Transit*, 220(3):219–234, 2006.

[18] K L Johnson. *Contact Mechanics*. Cambridge University Press, 1985.

[19] Computational Mechanics Beasy. Technical manual. Ashurst Lodge, Ashurst, Southampton SO40 7AA, UK, 2006.

[20] F Erdogan and G C Sih. On the crack extension in plates under plane loading and transverse shear. *ASME Journal of Basic Engineering*, (85):519–525, 1963.

[21] M Kaneta and Y Murakami. Propagation of semi-ellitpical surface cracks in lubricated rolling/sliding elliptical contacts. *ASME Journal of Tribology*, 113:270–275, 1991.

[22] P E Bold, M W Brown, and R J Allan. Shear mode crack growth and rolling contact fatigue. *Wear*, 144:307–317, 1991.

Appendix

Beasy & 2.5d model results, including residual stress

Table 2 in Section 4.2 shows the conditions modelled using a three dimensional model in Beasy for cases including residual stress. This Appendix includes a full set of the results generated, plotted as stress intensity factor variation for a crack located at the origin as a wheel contact moves across. Mode I stress intensity factor was predicted to be zero for all cases modelled using Beasy with residual stress included in the model, so only mode II results are plotted here.

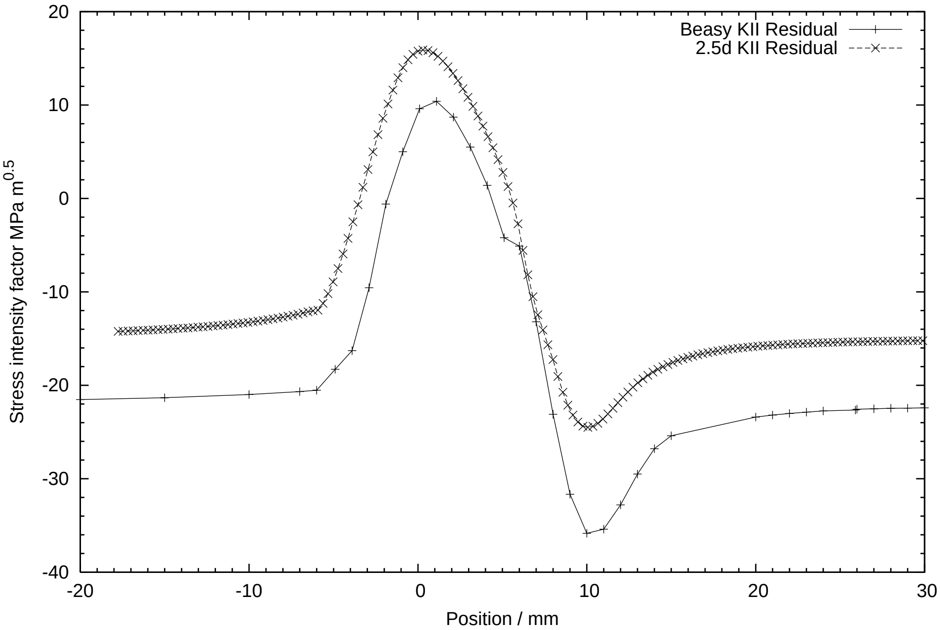

(a)

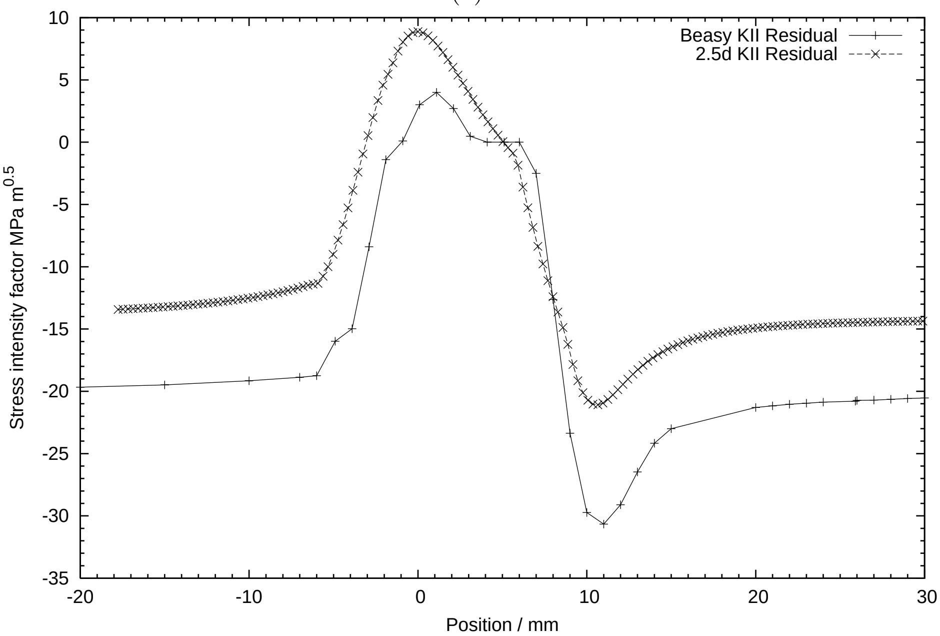

(b)

Figure 23: Mode II Beasy and comparable 2.5d modelling results for a 5mm radius crack. (a) $\mu_{surface} = 0.15$, $\mu_{crack} = 0.05$. (b) $\mu_{surface} = 0.15$, $\mu_{crack} = 0.15$.

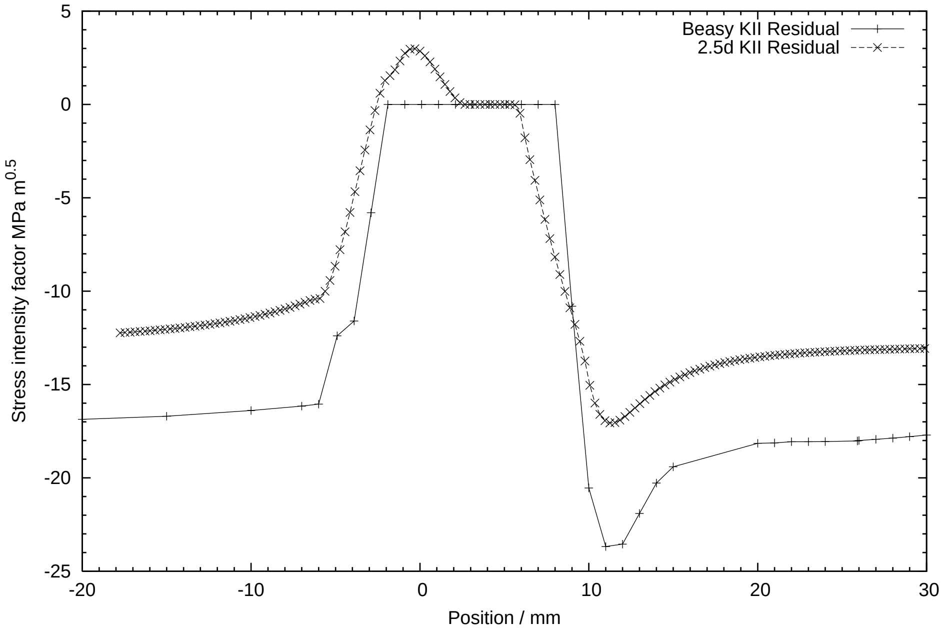

(a)

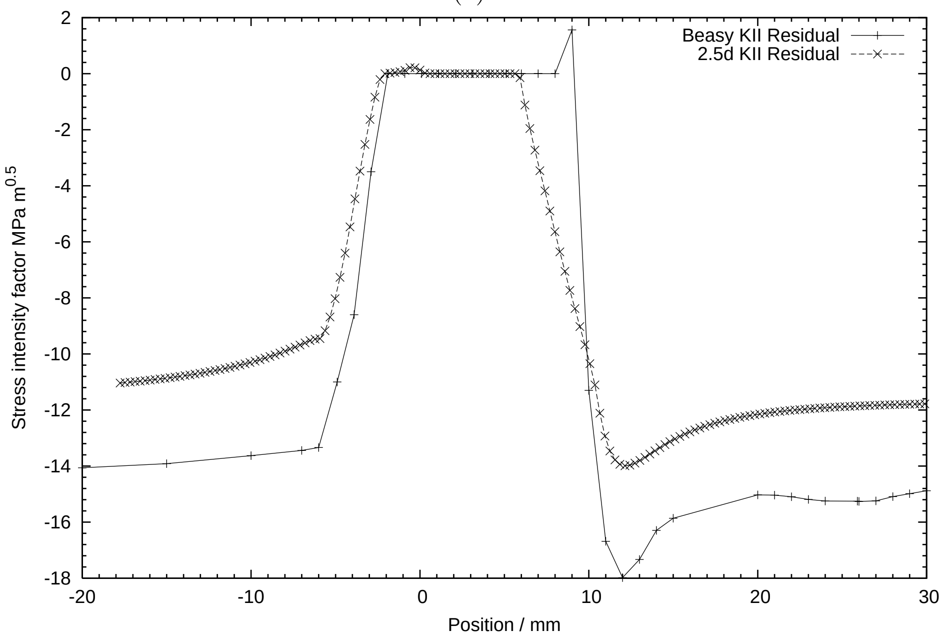

(b)

Figure 24: Mode II Beasy and comparable 2.5d modelling results for a 5mm radius crack. (a) $\mu_{surface} = 0.15$, $\mu_{crack} = 0.30$. (b) $\mu_{surface} = 0.15$, $\mu_{crack} = 0.45$.

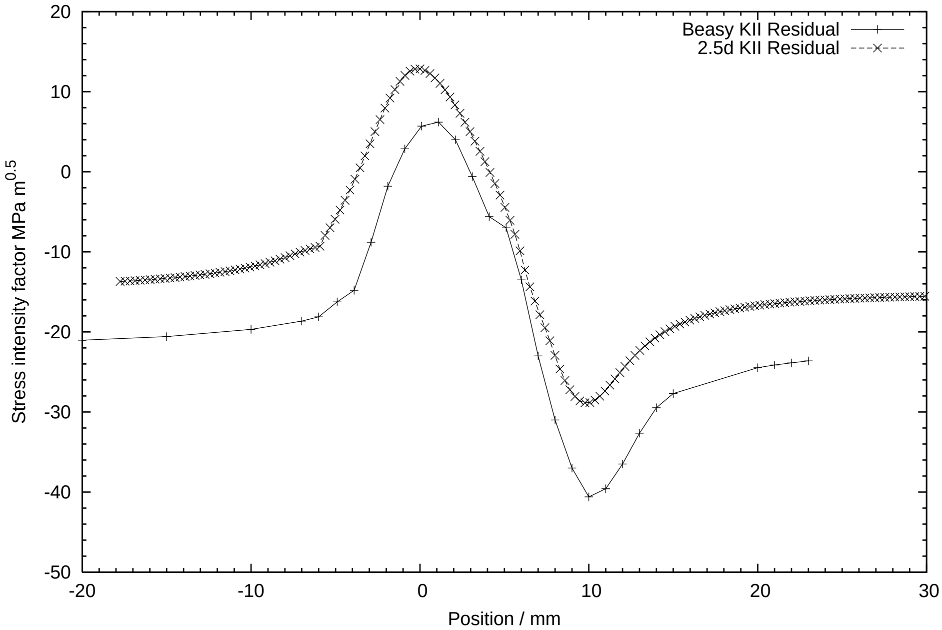

(a)

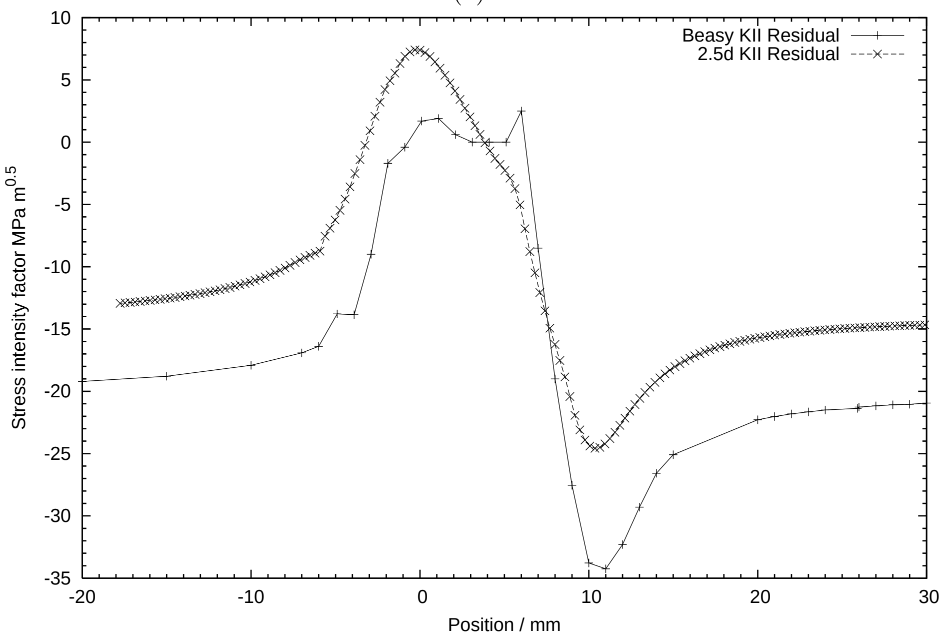

(b)

Figure 25: Mode II Beasy and comparable 2.5d modelling results for a 5mm radius crack. (a) $\mu_{surface} = 0.30$, $\mu_{crack} = 0.05$. (b) $\mu_{surface} = 0.30$, $\mu_{crack} = 0.15$.

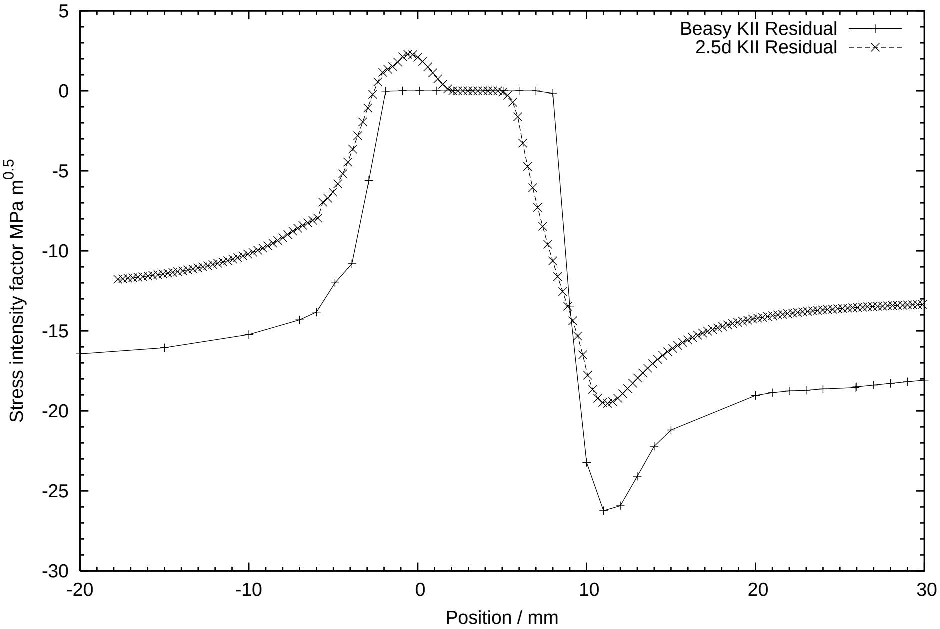

(a)

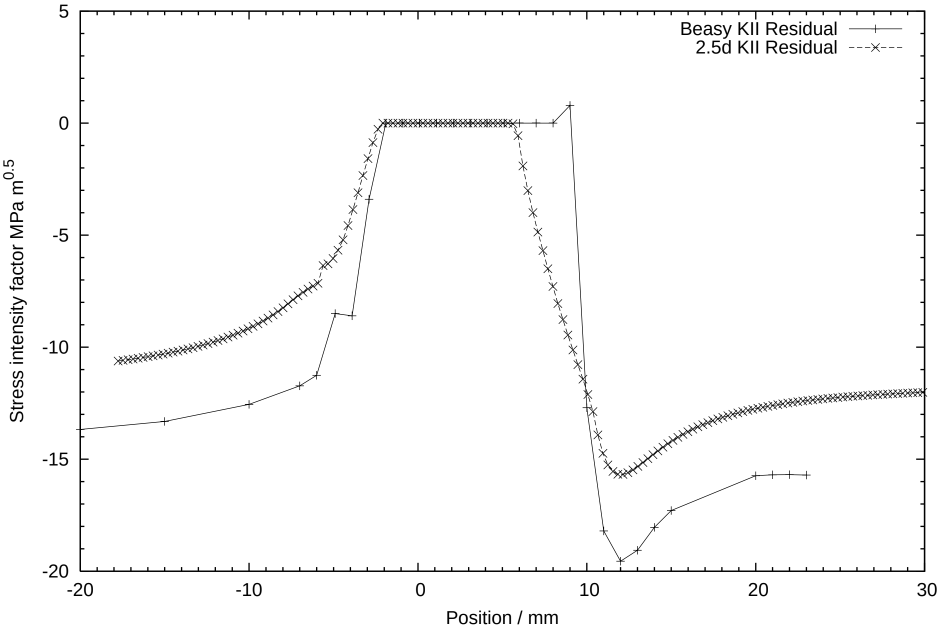

(b)

Figure 26: Mode II Beasy and comparable 2.5d modelling results for a 5mm radius crack. (a) $\mu_{surface} = 0.30$, $\mu_{crack} = 0.30$. (b) $\mu_{surface} = 0.30$, $\mu_{crack} = 0.45$.

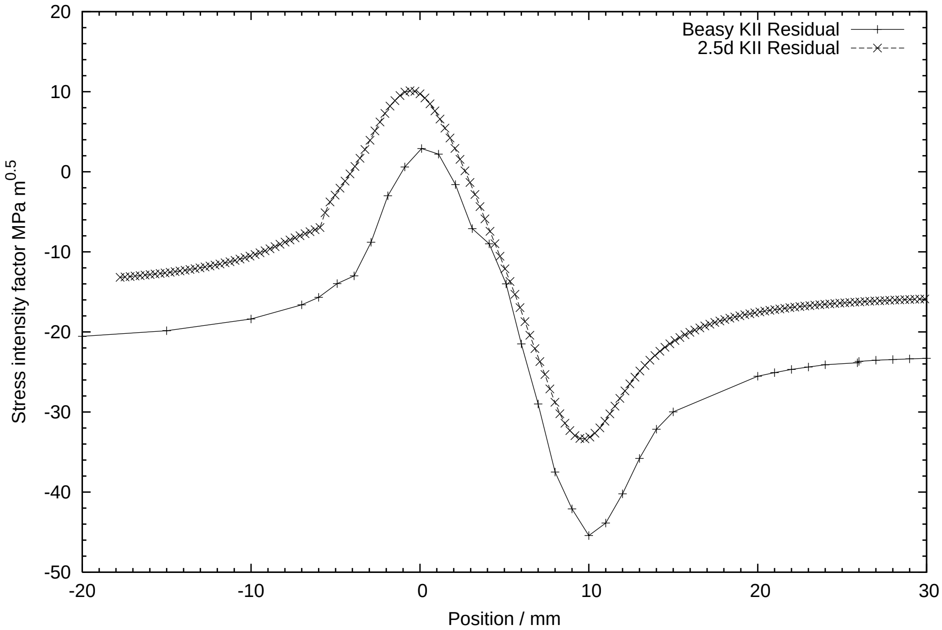

(a)

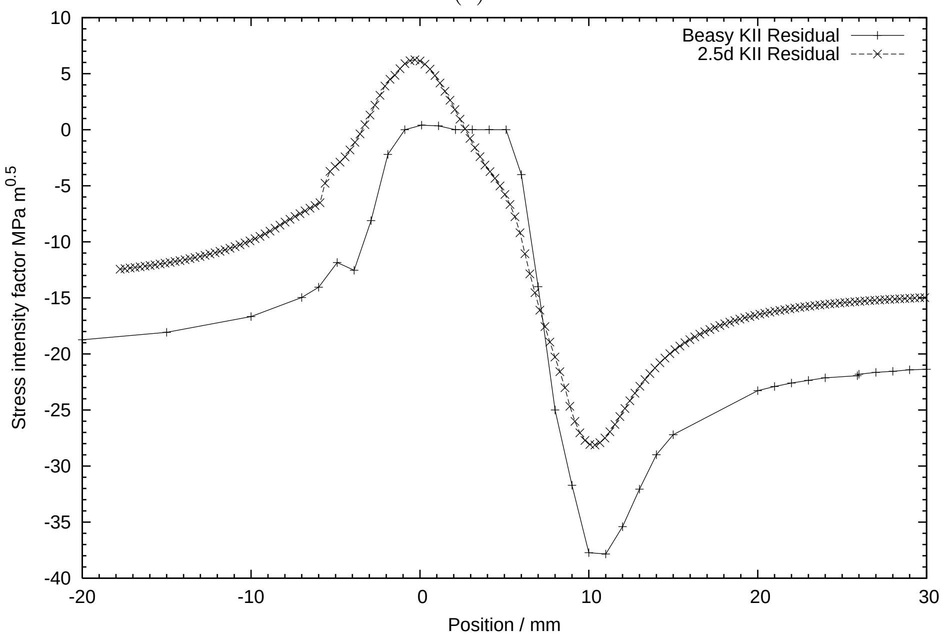

(b)

Figure 27: Mode II Beasy and comparable 2.5d modelling results for a 5mm radius crack. (a) $\mu_{surface} = 0.45$, $\mu_{crack} = 0.05$. (b) $\mu_{surface} = 0.45$, $\mu_{crack} = 0.15$.

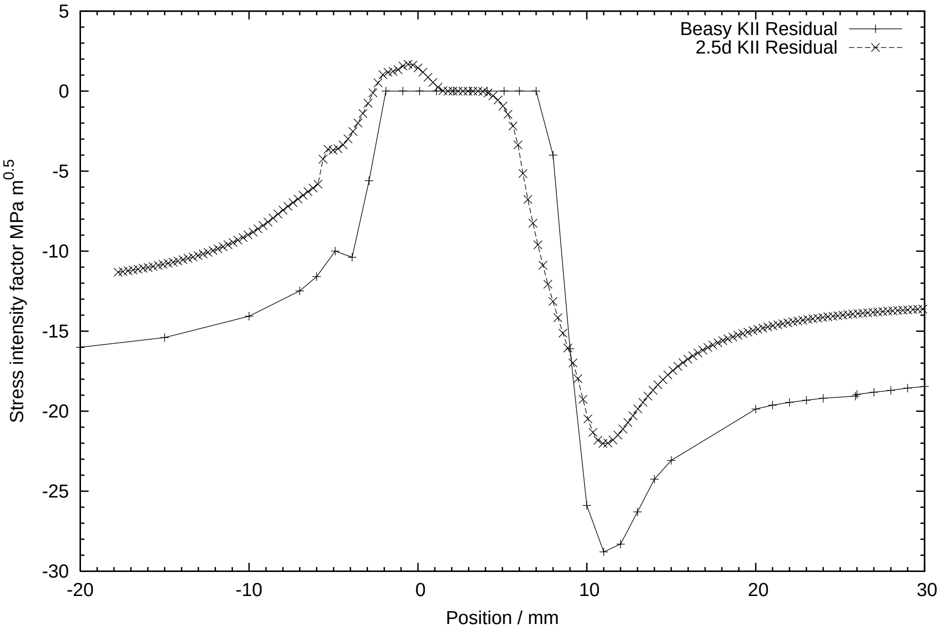

(a)

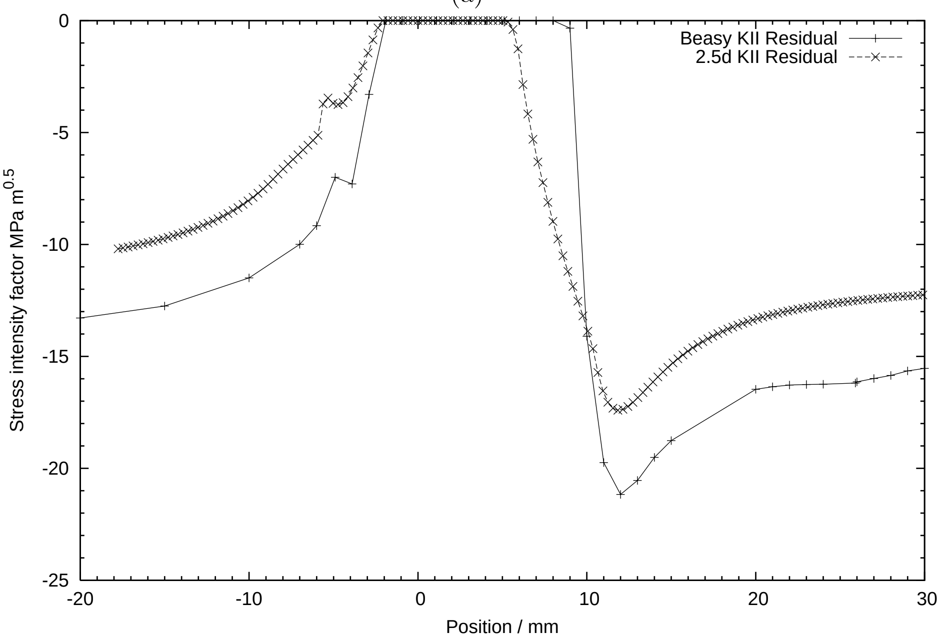

(b)

Figure 28: Mode II Beasy and comparable 2.5d modelling results for a 5mm radius crack. (a) $\mu_{surface} = 0.45$, $\mu_{crack} = 0.30$. (b) $\mu_{surface} = 0.45$, $\mu_{crack} = 0.45$.

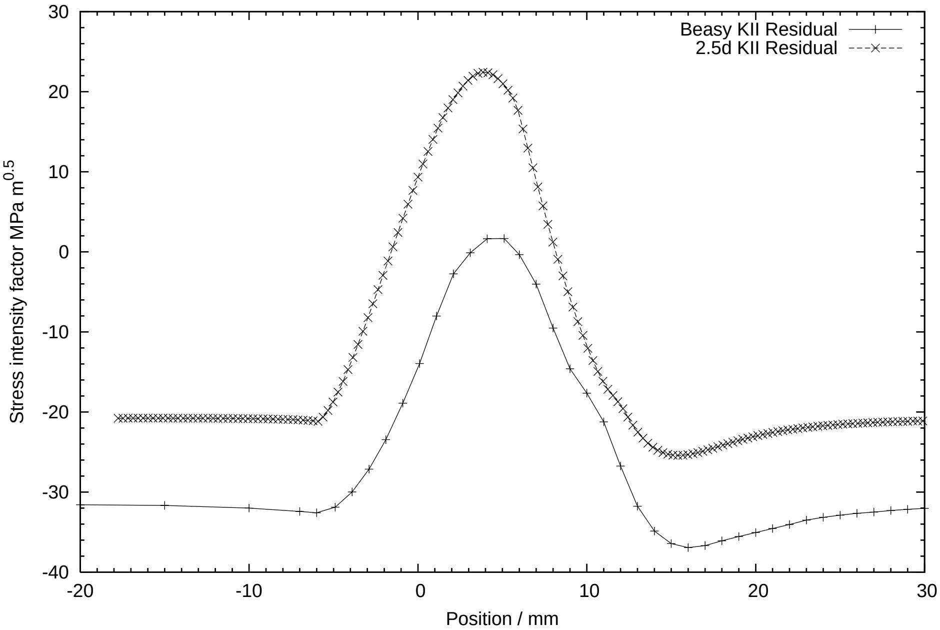

(a)

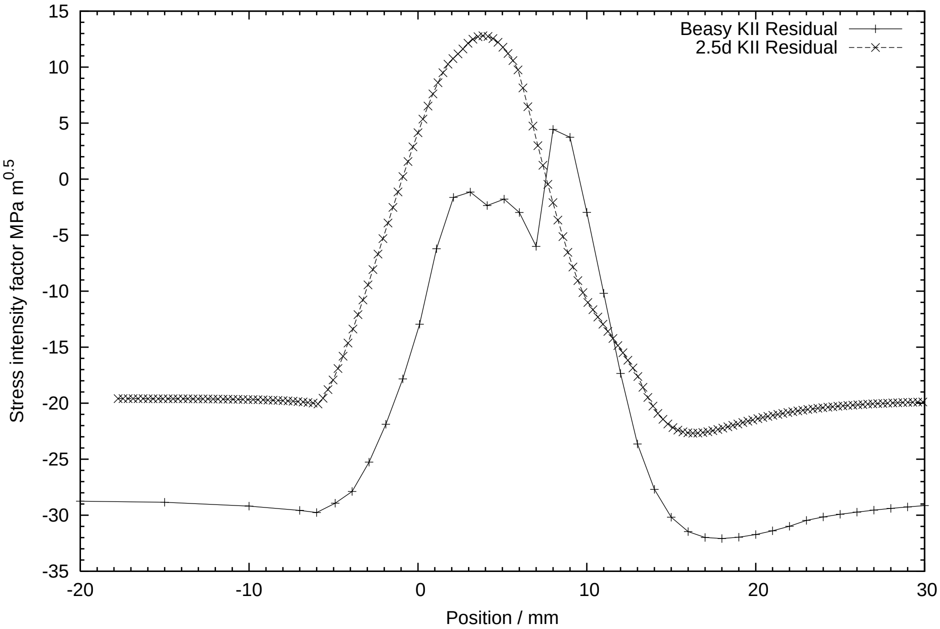

(b)

Figure 29: Mode II Beasy and comparable 2.5d modelling results for a 10mm radius crack. (a) $\mu_{surface} = 0.00$, $\mu_{crack} = 0.05$. (b) $\mu_{surface} = 0.00$, $\mu_{crack} = 0.15$.

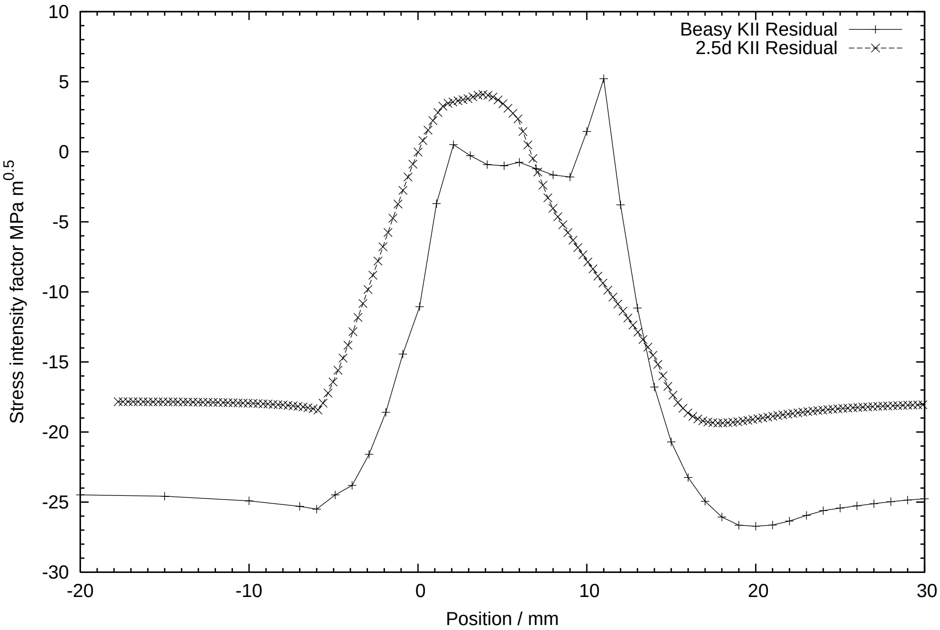

(a)

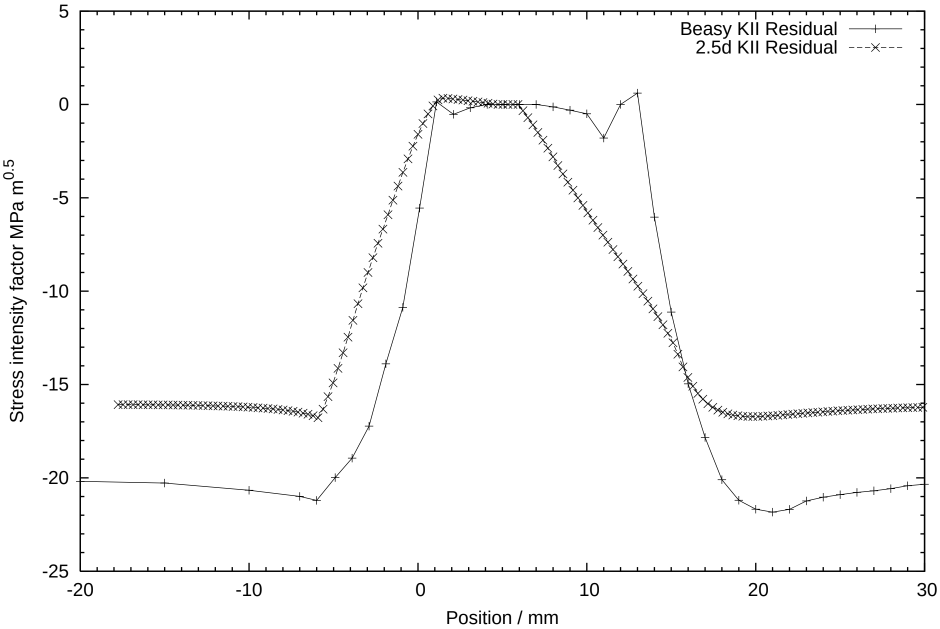

(b)

Figure 30: Mode II Beasy and comparable 2.5d modelling results for a 10mm radius crack. (a) $\mu_{surface} = 0.00$, $\mu_{crack} = 0.30$. (b) $\mu_{surface} = 0.00$, $\mu_{crack} = 0.45$.

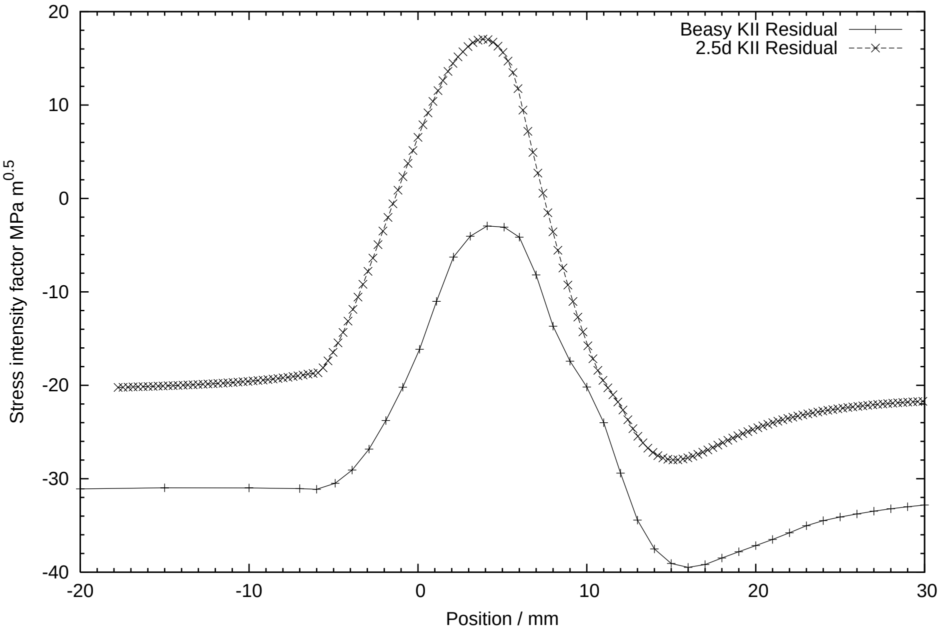

(a)

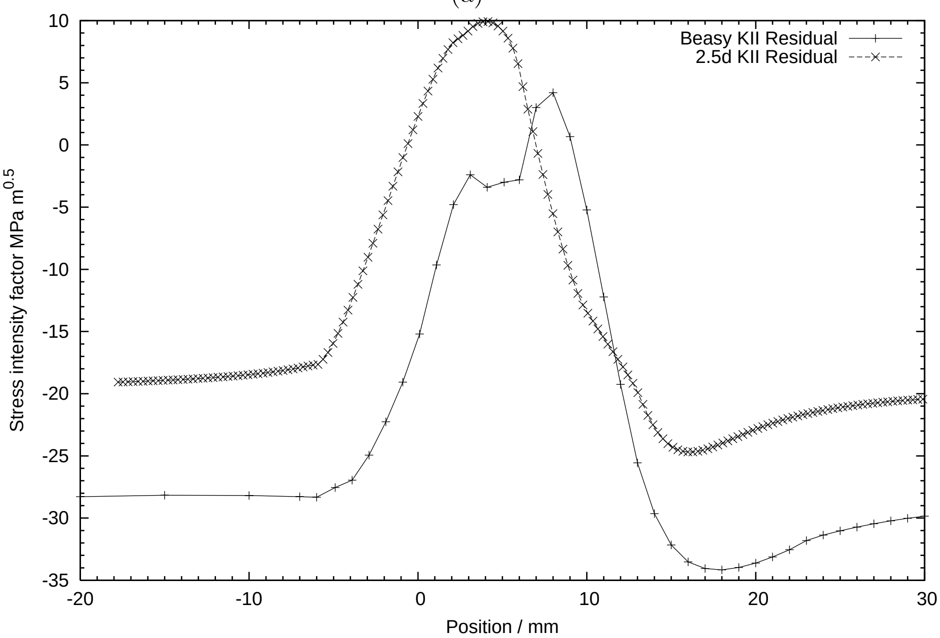

(b)

Figure 31: Mode II Beasy and comparable 2.5d modelling results for a 10mm radius crack. (a) $\mu_{surface} = 0.15$, $\mu_{crack} = 0.05$. (b) $\mu_{surface} = 0.15$, $\mu_{crack} = 0.15$.

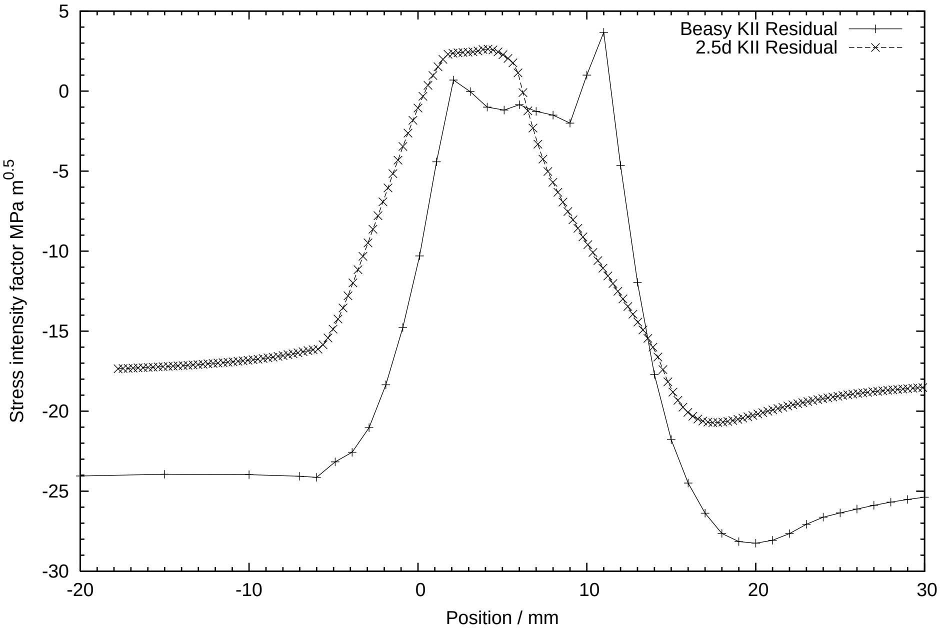

(a)

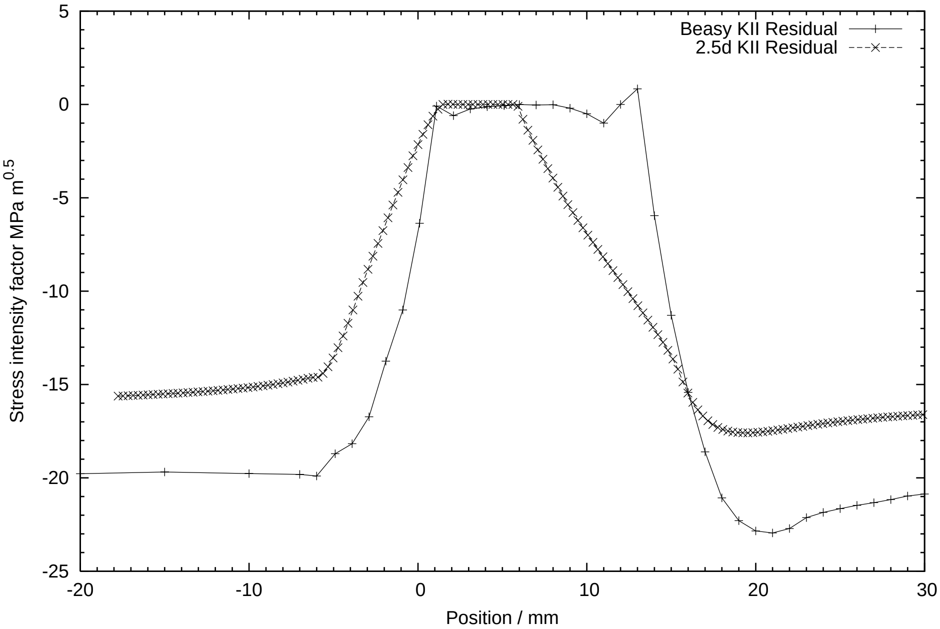

(b)

Figure 32: Mode II Beasy and comparable 2.5d modelling results for a 10mm radius crack. (a) $\mu_{surface} = 0.15$, $\mu_{crack} = 0.30$. (b) $\mu_{surface} = 0.15$, $\mu_{crack} = 0.45$.

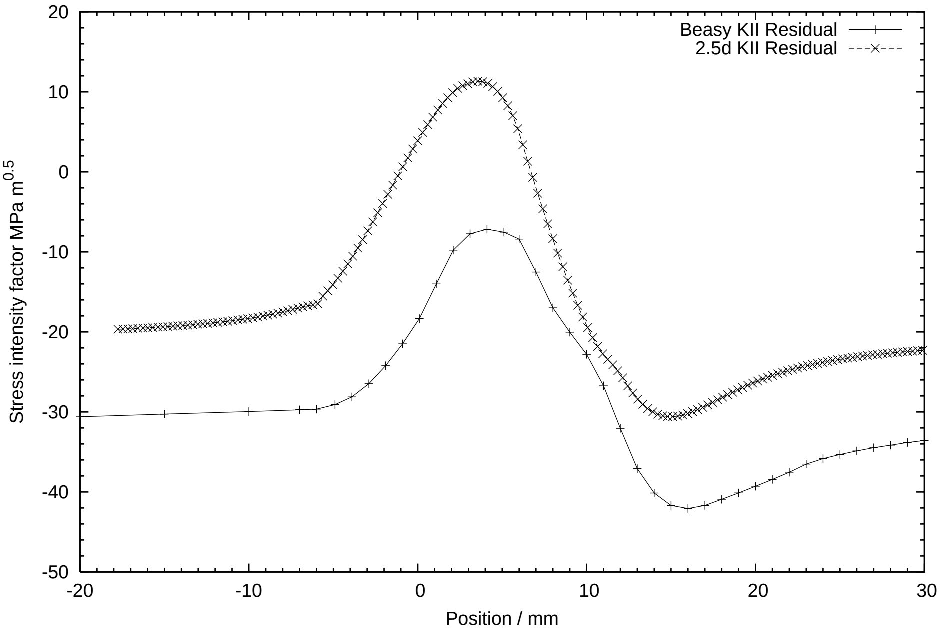

(a)

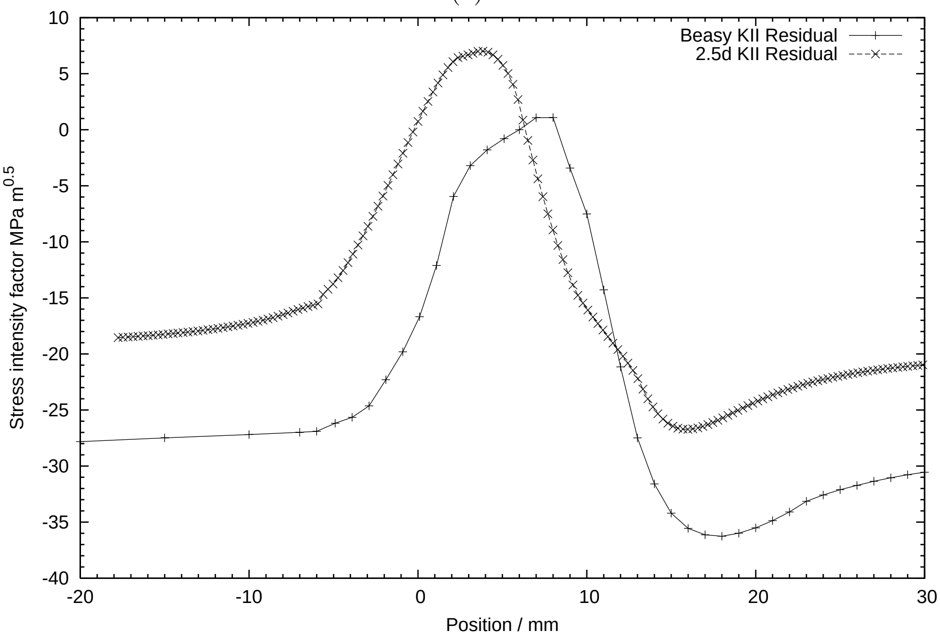

(b)

Figure 33: Mode II Beasy and comparable 2.5d modelling results for a 10mm radius crack. (a) $\mu_{surface} = 0.30$, $\mu_{crack} = 0.05$. (b) $\mu_{surface} = 0.30$, $\mu_{crack} = 0.15$.

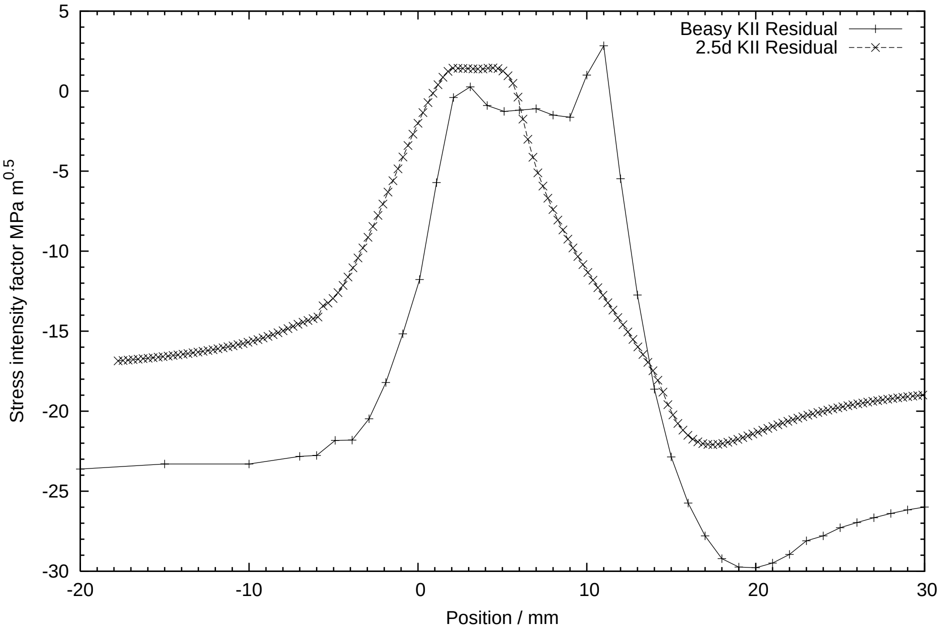

(a)

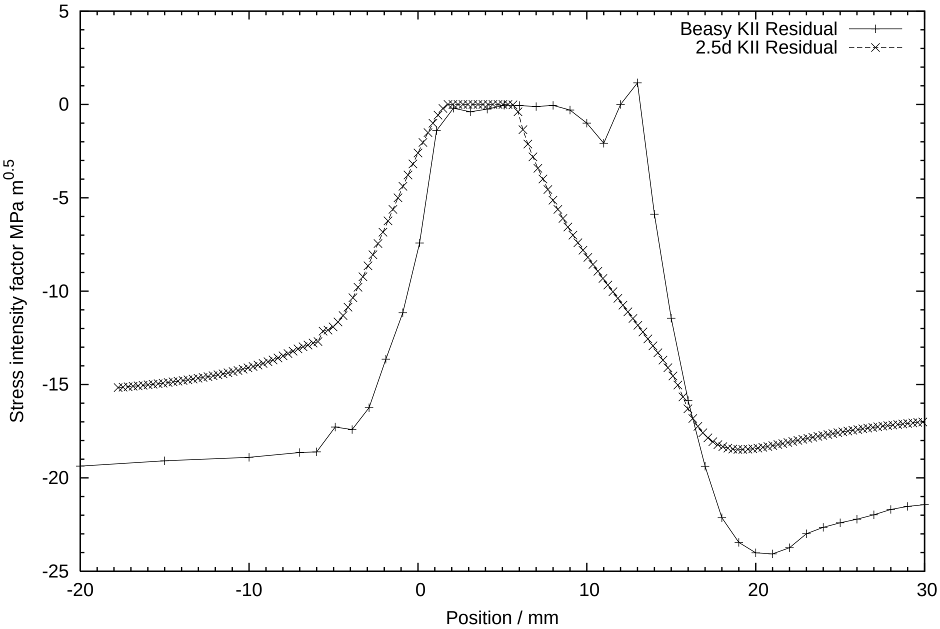

(b)

Figure 34: Mode II Beasy and comparable 2.5d modelling results for a 10mm radius crack. (a) $\mu_{surface} = 0.30$, $\mu_{crack} = 0.30$. (b) $\mu_{surface} = 0.30$, $\mu_{crack} = 0.45$.

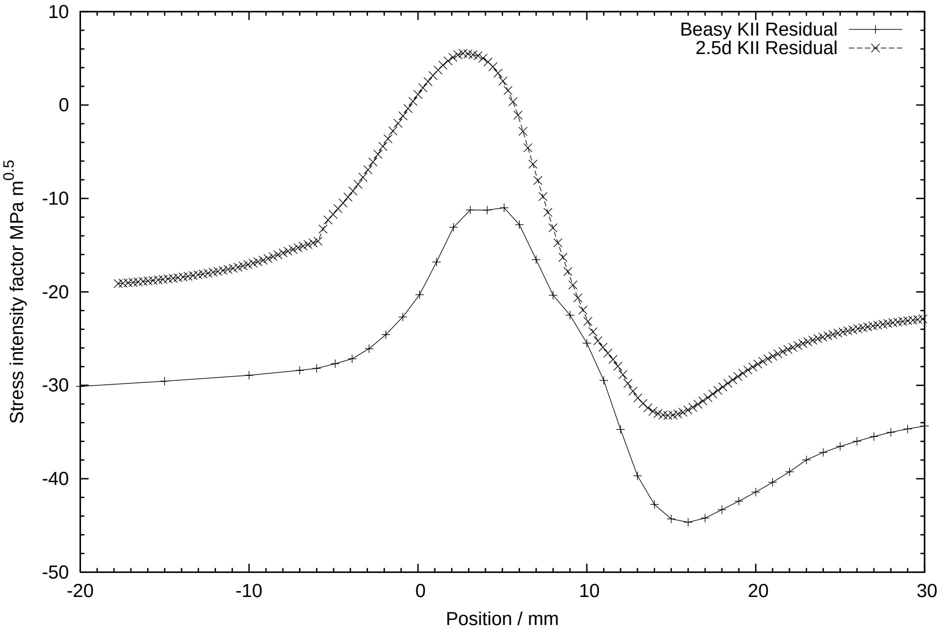

(a)

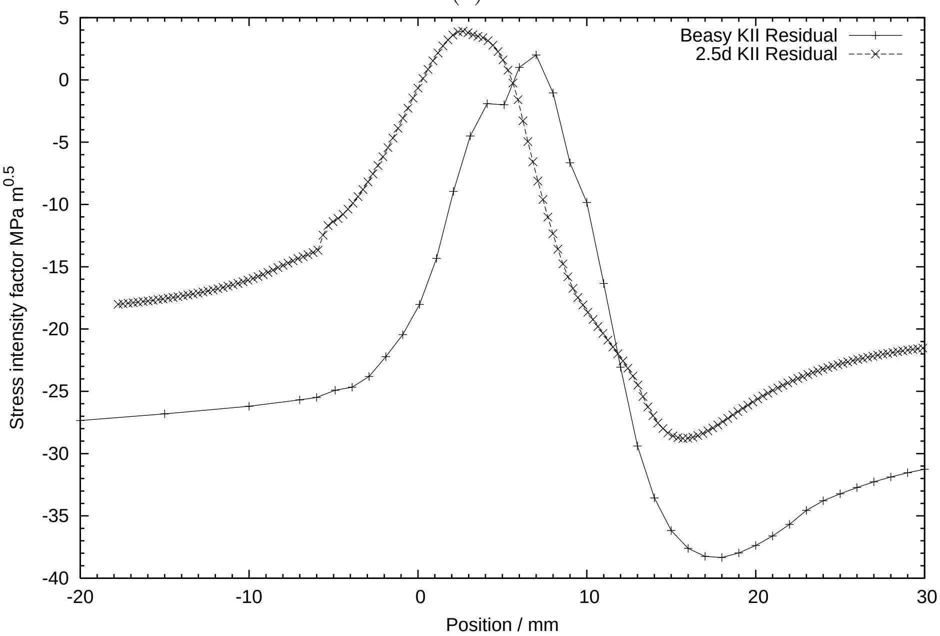

(b)

Figure 35: Mode II Beasy and comparable 2.5d modelling results for a 10mm radius crack. (a) $\mu_{surface} = 0.45$, $\mu_{crack} = 0.05$. (b) $\mu_{surface} = 0.45$, $\mu_{crack} = 0.15$.

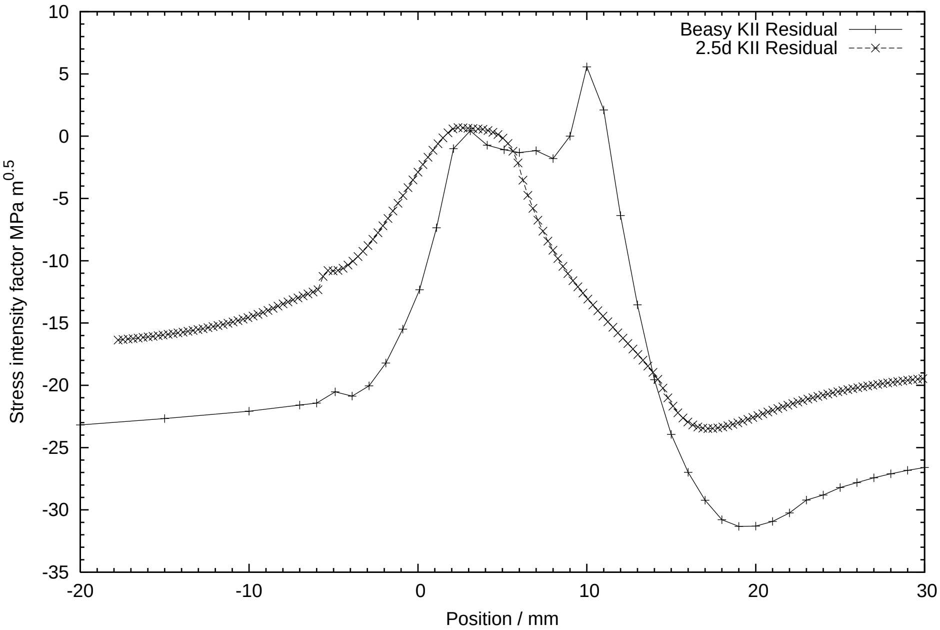

(a)

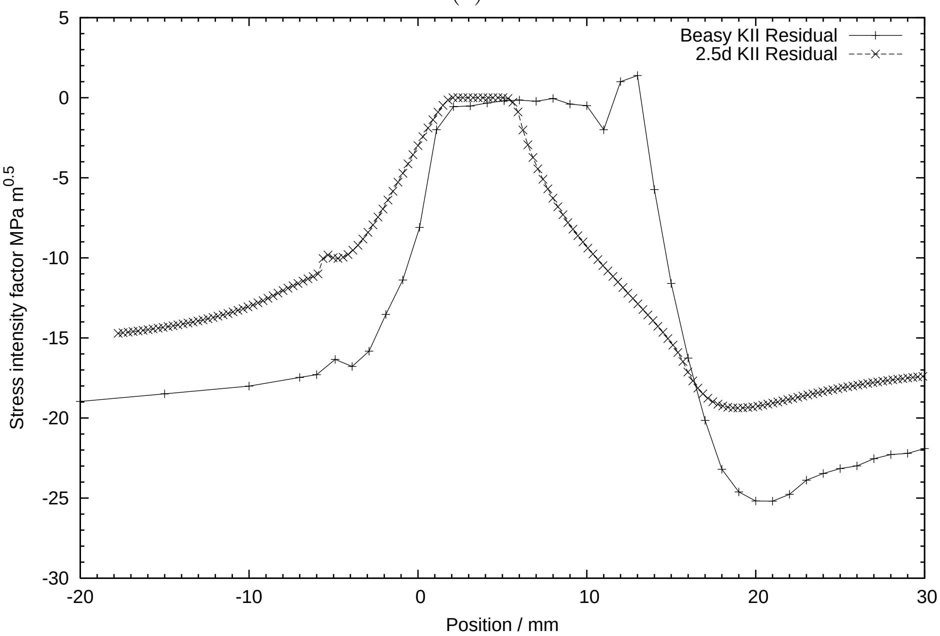

(b)

Figure 36: Mode II Beasy and comparable 2.5d modelling results for a 10mm radius crack. (a) $\mu_{surface} = 0.45$, $\mu_{crack} = 0.30$. (b) $\mu_{surface} = 0.45$, $\mu_{crack} = 0.45$.